Patterns of Wood and Sediment Storage Along Debris-flow Impacted Headwater Channels in Old-Growth and Industrial Forests

Jeremy T. Bunn

A thesis submitted in partial fulfillment of the
requirements for the degree of

Master of Science

University of Washington

2003

Program Authorized to Offer Degree: Department of Earth and Space Sciences

University of Washington
Graduate School

This is to certify that I have examined a copy of a master's thesis by

Jeremy T. Bunn

and have found that it is complete and satisfactory in all respects,
and that any and all revisions required by the final
examining committee have been made.

Committee Members:

_____
David R. Montgomery

_____
Jeffrey D. Parsons

_____
Joanne Bourgeois

Date: _____

In presenting this thesis in partial fulfillment of the requirements for a Master's degree at the University of Washington, I agree that the Library shall make its copies freely available for inspection. I further agree that extensive copying of this thesis is allowable only for scholarly purposes, consistent with "fair use" as prescribed in the U.S. Copyright Law. Any other reproduction for any purposes or by any means shall not be allowed without my written permission.

Signature: _____

Date: _____

University of Washington

Abstract

Patterns of Wood and Sediment Storage Along Debris-flow Impacted Headwater Channels in Old-Growth and Industrial Forests

Jeremy T. Bunn

Chair of the Supervisory Committee:
Professor David R. Montgomery
Department of Earth and Space Sciences

I investigated the effect of hillslope forest conditions and in-channel large woody debris (LWD) on channel sediment storage and sediment delivery by debris flows, using a combination of aerial photograph interpretation and field surveys to compare the characteristics of wood-rich and wood-poor debris-flow tracks in old-growth and industrial forests of the western Olympic Peninsula. Debris-flow initiation sites are more than four times as common in the industrial forest as in the old-growth, and debris-flow density is three times greater in the industrial forest. Along recent debris-flow tracks in both forest types over 75% of retained sediment is in contiguous deposits upstream of LWD. The volume of sediment and wood in old-growth is 5 to 11 times greater than in industrial-forest channels. The difference in sediment retention leads to a greater proportion of exposed bedrock in channels flowing through industrial forest. In old-growth forest, large-volume sediment deposits were common in even the steepest surveyed reaches. Most of the sediment-retaining LWD in both forest types is of a diameter greater than is likely to be provided by forests that are clear-cut in short rotation. Short-rotation clearing of forest from the hillsides of headwater basins and removal of old-growth LWD from headwater channels should be expected to result in a landscape with thinner hillslope soils and less sediment storage in headwater channels, leading to a system in which sediment output to higher-order channels is more tightly coupled to the rate of sediment production on hillslopes.

TABLE OF CONTENTS

LIST OF FIGURES

LIST OF TABLES

Acknowledgements

I wish to express my gratitude to Dave Montgomery for providing inspiration, support, and constructive criticism, and to Jody Bourgeois and Jeff Parsons for their insightful comments and helpful suggestions. Bill Baccus facilitated the work in Olympic National Park. Harvey M. Greenberg provided GIS data and assistance. Special thanks go to Byron Amerson, Suzanne Osborne, Dave Trippett, Peter Wald, Chris Brummer, Pam Hartman, Simon DeSzoeke, Suzaynn Schick, and Oliver Deschler for providing invaluable assistance during sometimes difficult and hazardous fieldwork. This research was supported by USDA Forest Service Cooperative Agreement # PNW 99-3032-2-CA and the University of Washington Department of Earth and Space Sciences.

1. INTRODUCTION

In comparison to the large number of studies of sediment transport and reach-scale morphology in low-gradient alluvial channels, relatively little work has been done in steep mountain channels [*Wohl*, 2000]. Even less work has focused on debris-flow-prone headwater streams. This relatively neglected portion of channel networks is nonetheless significant; it includes most of the total channel length in a channel network [*Shreve*, 1969] and most of the drainage area in mountain drainage basins [*Sidle et al.*, 2000]. Headwater channels (and their adjacent hillslopes) are also the source of much of the sediment and woody debris that enters the fluvial system. Consequently there is growing interest in the physical and biological processes that occur in headwater channels [e.g., *Dieterich and Anderson*, 1998; *May*, 2001, 2002; *Sidle et al.*, 2000; *Gomi et al.*, 2002].

The processes affecting headwater streams are linked to processes affecting adjacent hillslopes [*Church*, 2002; *Gomi et al.*, 2002]. Sediment transport and channel geometry in headwater streams are dominated by landslide-triggered debris flows rather than by fluvial transport [*Swanson and Swanston*, 1977; *Benda*, 1990; *Seidl and Dietrich*, 1992; *Gomi et al.*, 2002]. It has been widely reported that debris flows scour the channels through which they travel, transporting sediment and woody debris to distinct deposition zones [e.g., *Gomi et al.*, 2002]. Although much of the early research on debris flows was undertaken in industrial (i.e., clear cut) forests, recent

work has begun to document the ways that debris flow activity differs between old-growth and industrial forests.

Several studies have demonstrated that landslides and/or debris flows are more common or frequent in industrial forests than in old-growth forests. *Morrison* [1975, as cited in *May*, 2002] found debris flow frequency to be 8.8 times higher in clear-cuts than in forested areas. Various studies cited by *Johnson et al.* [2000] found a two- to fourfold increase in landslide frequency associated with timber harvest. *Snyder* [2000] found three times more debris flow initiation sites in timber plantations than in old-growth forests. *May* [2002] found landslide density to be four times higher in second growth forest and ten times higher in clear-cuts than in old-growth forest.

Large woody debris (LWD) is known to affect reach-scale morphology and hydrological and sediment-transport processes in alluvial channels [*Bugosh and Custer*, 1989; *Montgomery et al.*, 1995; *Fetherston et al.*, 1995; *Abbe and Montgomery*, 1996, 2003]. Some studies have found that there are more pieces of LWD in old-growth streams than in those flowing through clear-cut forests [*Murphy and Koski*, 1989; *Bilby and Ward*, 1991; *McHenry et al.*, 1998]. Others have found that there is more woody debris in logged streams [*Froehlich*, 1973; *Gomi et al.*, 2001] and one study found no significant difference in number of pieces of LWD between harvested and unharvested streams [*Ralph et al.*, 1994]. Log jams are known to retain sediment in both low gradient and steep headwater channels [*Perkins*, 1989;

O'Connor, 1994; *Montgomery et al.*, 1996], and it has been hypothesized that incorporation of LWD into the leading edge of debris flows may result in deposition in steep portions of the channel network [*Montgomery and Buffington*, 1998; *Lancaster et al.*, 2001]. *May* [1998] found that runout distance tends to be greater for debris flows that originate in or travel through clear-cut industrial forest in the Oregon Coast Range, perhaps reflecting LWD-forced deposition closer to debris flow initiation sites in old-growth forest.

Differences in hillslope forest condition and in-channel LWD between old-growth and industrial forests may lead to differences in landscape-scale debris flow activity and reach-scale morphology, sediment transport, and sediment storage. Recent studies of headwater channels in the Oregon Coast Range and British Columbia [*May*, 1998, 2002; *Johnson et al.*, 2000; *Gomi et al.*, 2001] provide some of the relatively few data sets available that address the effects of forest type and LWD on debris flow processes and the nature of headwater channels in the Pacific Northwest. Using a combination of aerial-photograph interpretation, field surveys, and theoretical-model exploration, I investigated the effect of hillslope forests and in-channel LWD on sediment storage and transport by debris flows at both channel and basin scales in the western Olympic mountains of Washington. The objectives of my research were a) to complement earlier efforts by extending the geographical range of existing studies, and b) to propose causal explanation(s) for observed differences in debris flow processes between old-growth and industrial forest.

2. METHODS

2.1. Study Area

Located on the western flank of the Olympic Mountains, the study area (Figure 1, page 12) is characterized by east-west trending ridges with steep, forested hillslopes that descend to wide glacially carved valleys. Like much of the forested mountain terrain of the Pacific Northwest, these hillslopes are subject to erosion by mass wasting [*Schlichte*, 1991]. The aerial photograph survey covered portions of the Calawah, Bogachiel, Hoh, Clearwater, and Queets drainage basins. Study area boundaries were chosen to straddle the border between 1) old-growth forest within Olympic National Park (ONP) and 2) Washington State Department of Natural Resources (WADNR) and Forest Service lands that have been subject to timber harvest. Drainage basins on either side of the ONP boundary are similar with respect to parameters such as precipitation, channel network topology, drainage area, elevation, relief and geological substrate that are likely to affect landsliding and debris flows [*Selby*, 1993]. Annual precipitation ranges from 4 m to 5 m and falls primarily as rain between September and June [*Heusser*, 1974]. Elevation of the ridgelines ranges from 650 m to 1250 m, while main valley bottoms range from 120 m to 440 m. Local relief between ridgeline and valley bottom is typically between 650 and 700 m, but ranges from 500 m to 850 m. The valleys of the Western Olympic Mountains have experienced repeated glaciations during the Quaternary [*Heusser*, 1974] and

have a pinnate drainage pattern.

The drainage areas of the headwater basins in my study area range from 0.5 to 8.3 km^2. These small basins contain first- through third-order streams that flow from ridges of folded and faulted marine sandstone, siltstone, shale, and conglomerate [*Tabor and Cady*, 1978] down onto elevated terraces along the mainstem rivers. During my fieldwork I observed minor variation in lithology both within and between basins, but did not observe any consistent relationship between local variations in bedrock type and variations in channel form. Hillslope soils are gravelly loams, typically 0.5 to 1.5 m deep [*Schlichte*, 1991].

Old-growth forests in the region consist of western hemlock, Douglas-fir, western red cedar, Sitka spruce, and various understory species [*Edmonds*, 1998]. The industrial forests that I visited consist almost entirely of even aged stands of Douglas-fir, with a dense understory of devil's club, huckleberry and vine maple wherever the conifer canopy is thin. Digital elevation model (DEM) analysis and field observations indicate that slopes range from less than 1% on the valley bottoms to nearly vertical along the inner gorges of some creeks. Most of the primary forest has been harvested from the private, state, and tribal lands of the Olympic peninsula [*Peterson et al.*, 1997], but old-growth forest has been preserved within the boundaries of Olympic National Park. Industrial forestry in the western Olympic Mountains has thus set up a large-scale perturbation experiment [as defined by *Ford*, 2000], in which basins within the park serve as controls, and the similarities in lithology, slope, weather and

climate allow comparison between headwater channels in industrial and old-growth forests.

2.2. Aerial Photograph Survey Methods

I identified slope failures and debris flow tracks on aerial photograph stereopairs and mapped them to digital orthophotos using ArcView [ESRI, 1999]. The original photographs are 1:32,000 scale, and were viewed through 3x magnification. Photographs of the entire study area at this resolution were only available from the most recent WADNR survey (OL-QT-00, flown in 2000), so I limited my survey to this one set. I mapped debris flow tracks at three defined confidence levels. "High" confidence level required that I observed a visible head scarp, open canopy along the presumed runout path, and a visible deposition lobe. "Medium-confidence" required an open canopy track with either a visible head scarp or deposition lobe. Where I observed only an open canopy track I classified the suspected debris flow track as "low-confidence". Forty percent of the mapped debris flow tracks were high-confidence, 50% were medium-confidence, and 10% were low-confidence. Over 95% of the features I mapped were $\geq$ 50 m long.

To investigate landscape-scale differences in the rate and spatial extent of debris flow activity I compared the area inside ONP (old-growth forest) and the area outside of the park (industrial forest) with respect to five parameters: primary runout length (R_P), cumulative runout length (R_C), debris flow density (D_{DF}), dimensionless debris flow density (D_{DF}*), defined as the ratio of debris flow density to drainage density,

and spatial frequency of debris flow initiation (I_{DF}). I used the definitions of primary and cumulative runout length suggested by *May* [2002], in which R_P is the length of the longest single-line debris flow track, and R_C is the total length of debris flow tracks in a basin. D_{DF} was defined as the total length of debris flow tracks divided by the area over which they were summed. I therefore obtained both primary and cumulative debris flow densities for each forest type. To facilitate calculation of D_{DF}* I used the FLOW module in IDRISI [Clark Labs, 2002] to derive a drainage network from a 10-meter-grid DEM of the study area created by compositing individual DEMs from U.S. Geological Survey 7.5' quadrangles. I set the drainage area for channel initiation to 25,000 m^2 to minimize the generation of DEM-artifact channels [Jonathan Stock, personal communication]. To control for different proportions of upland in the old-growth and industrial-forest parts of the study area I subtracted the mainstem valley floors from the map area used to calculate D_{DF} and D_{DF}*. I defined I_{DF} as the number of debris-flow-initiating scarps divided by the area over which they were summed. To calculate I_{DF} I counted the number of mapped slope failure sites in each forest class and divided that number by the corresponding upland area.

2.3. Field Survey Methods

I performed detailed field surveys of a subset of the mapped debris flows, selected on the basis of "high confidence" identification in my aerial photograph mapping and

accessibility from road or trail. I surveyed four debris flows inside the park and one outside the park that traveled through old-growth forest, four outside the park that traveled through industrial forest, and one outside the park that traversed both old-growth and industrial stands (Table 1, page 12). I used stadia rod, 100 m fiberglass tape, Abney level, laser rangefinder, and Brunton compass to map and survey the long profile of each debris flow track. I started my surveys where there was either loss of valley confinement or channel slope $\approx$ 10%, along with clear evidence of terminal debris flow deposition (the development of a distinct fan). Surveys continued upstream until I reached the initiating scarp or an impassable waterfall. At 5 to 20 m intervals (depending on morphological complexity) along the length of each debris flow track I recorded downstream bearing, elevation change, bed width, bed material, sediment depth (where it could be observed), the composition of sideslope cover within 5 m vertical distance of the channel bed, the volume and type of sideslope sediment deposits, and the diameter, length, and alignment with respect to channel centerline of functioning large woody debris (LWD_F), defined as any piece of wood that was either shielding or damming a distinct volume of sediment that formed a step $\geq$ 0.5 m above the adjacent bed.

I characterized bed material as either bedrock or some combination of gravel (5 mm to 75 mm), cobbles (75 mm to 300 mm), boulders (>300 mm), and/or LWD. Wood was considered to be a bed material when a noticeable proportion of the bed surface consisted of partially buried LWD such that a full bed-width discharge would flow

over it. I classified sideslope cover as bedrock, consolidated regolith, loose colluvium, or vegetation. To record the volume of sideslope sediment deposits I sketched simple abstractions of their shapes and measured the corresponding dimensions with a laser rangefinder. My method of sampling functional LWD was not exhaustive: where there were multiple pieces of LWD in a step-forming jam I measured only those that were in my judgment acting as key members, and I did not measure LWD that was retaining volumes of sediment smaller than about 2 m^3, so I may have underestimated the contribution of small pieces. I am confident, however, that I adequately sampled the LWD that was directly retaining sediment in the surveyed channels.

To estimate the volume of sediment stored in the channel I interpolated the bedrock surface between exposures to approximate sediment depth at each station (Figure 2, page 13), assumed a parabolic cross-sectional form, and calculated the sediment volume between stations as

$$V = \frac{L}{3}\left(W_0 D_0 + \tfrac{1}{2}\Delta W D_0 + \tfrac{1}{2}\Delta D W_0 + \tfrac{1}{3}\Delta W \Delta D\right) \qquad (1)$$

where V is sediment volume, L the horizontal distance between stations, W_0 is the bed width at the initial station, D_0 sediment depth at the initial station, ΔW is the change in bed width between stations, and ΔD the change in sediment depth between stations.

Volumes calculated using (1) are intermediate between those calculated using triangular and rectangular cross-sections and are more consistent with the observed

parabolic cross-sectional shape of bedrock channels in the field area. The derivation of (1) and details of the profile calculation and sideslope volume formulae are presented in the Appendices. Interpolation of the bedrock surface in places resulted in sediment depth ≤ 0 m for a channel segment where sediment was observed to be present (Figure 2). For these locations I substituted a depth of 0.4 m. This value is both consistent with sediment depths reported for Pacific Northwest channels by *Benda* [1988] and *May* [1998] and at the low end of the range of positive sediment depths calculated for the surveyed channels.

The accuracy of my estimates of sediment volume is limited by the necessity of interpolation between bedrock exposures along the channel profile. Since steeper reaches were often observed to have bedrock step morphology, it is possible that I have over- or underestimated sediment volumes by imposing a constant slope underneath sediment deposits (Figure 2). In any case, whatever bias exists is systematic across all sampled creeks, so relative comparison between creeks should be unaffected by possible misestimates of the true volumes.

I normalized the calculated sediment volume per unit length of channel to generate longitudinal sediment volume profiles for each surveyed creek. To investigate reach-scale properties I divided each channel into reaches of approximately 100 m length. The actual length of defined reaches varies between 74 and 138 m, since survey stations did not always fall on 100 m increments. For each reach I calculated the overall slope (the change in elevation divided by horizontal distance along the valley

centerline), the proportion of the length that was exposed bedrock, and the sediment volume normalized to unit lengths of 100 m.

2.4. Statistical Methods

I used the two-sided t-test for differences in means and two-sided F-test for differences in variances. Variables were log-transformed where necessary to obtain approximately normal distributions for hypothesis testing. To guard against pseudo-replication I compared the distribution of reach-scale parameters within each creek to the distribution across all creeks in its forest type. I found no significant channel effect and so considered each reach an independent sample for hypothesis testing.

TABLE 1. Surveyed Debris Flow Tracks

Creek Name	Abbreviation	Basin Area (km^2)	Last Debris flow	Surveyed Length (m)	Initiation	Runout
East Twin	ET	0.45	1997 [a]	565	Old-growth	Old-growth
Spawner	SP	1.24	2002 [b]	1480	Old-growth	Old-growth
West Twin	WT	1.07	1997 [a]	1139	Old-growth	Old-growth
Hoot	HR 5	1.23	1971-1990 [c]	907	Industrial	Old-growth
(?)	HBC	1.26	unknown	612	Industrial	Old-growth
Iron Maiden	HR 1	0.58	1981-1990 [c]	1596	Industrial	Both
(?)	HR 2	1.02	unknown	1193	Industrial	Industrial
Washout	HR 3	1.03	1981-1990 [c]	932	Industrial	Industrial
Dinky W.	HR 4	0.59	1971-1980 [c]	721	Industrial	Industrial
H-1070	HR 6	0.76	1981-1990 [c]	725	Industrial	Industrial

a. [Bill Baccus, personal communication]
b. inferred from posted date of trail washout
c. [*Schlichte*, 1991]

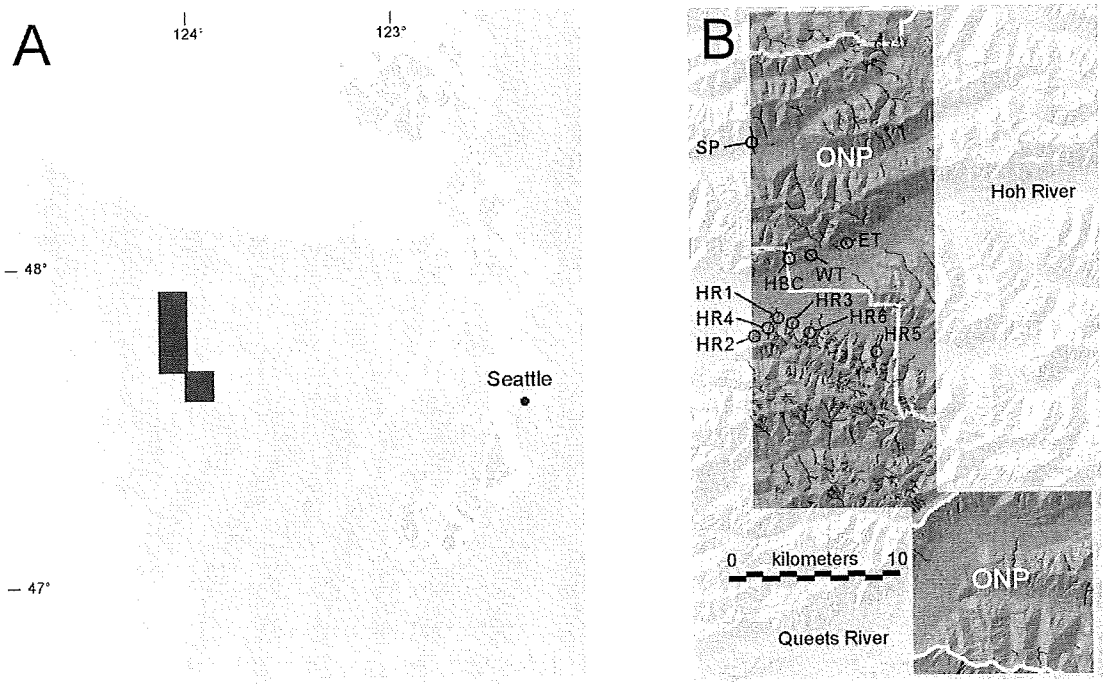

Figure 1: Location Maps. A: Map showing the location of the study area on the western side of the Olympic peninsula. B: Shaded relief map of the study area. Areas labeled ONP are within the boundaries of Olympic National Park. Black lines within the study area are mapped debris flow tracks. Field survey channels are labeled with their abbreviated name (refer to Table 1).

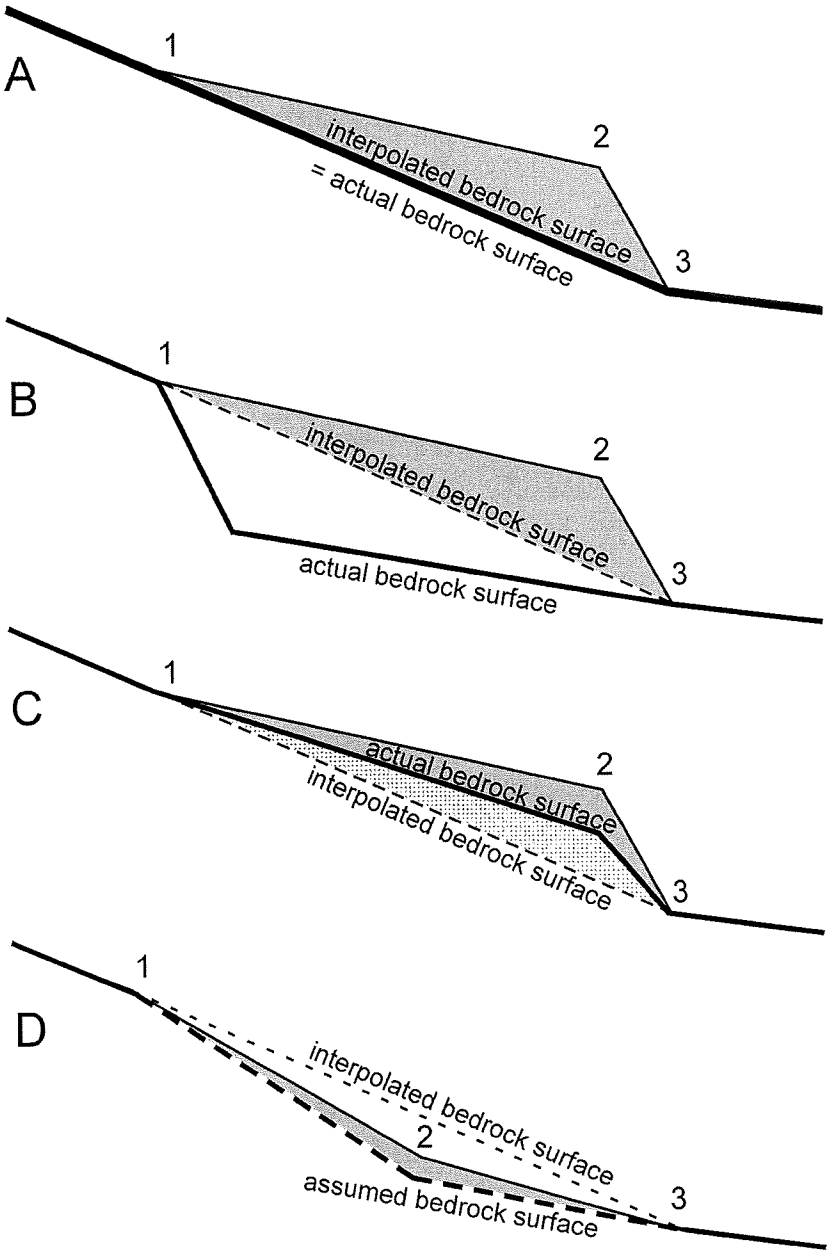

Figure 2: Sediment Depth Interpolation Between Stations. Stations 1, 2 and 3 record the upstream, intermediate, and downstream elevations of a sediment deposit.

A: Ideal sediment wedge: actual bedrock surface lies along interpolated line 1-3.

B: Problem – underestimation of sediment volume. Actual bedrock surface lies below interpolated line 1-3. Lighter grey fill represents uncounted sediment volume, which likely will at most equal counted volume.

C: Problem – overestimation of sediment volume. Actual bedrock surface lies above interpolated line 1-3. Lighter grey fill represents over-counted sediment volume.

D: Problem – interpolated line 1-3 results in nonsensical negative depth to sediment at 2. Depth of 0.4 meters substituted to yield approximate sediment volume.

3. RESULTS

3.1. Aerial Photograph Survey

In my study area debris flows were more common in the industrial forests outside of ONP than they were in the old-growth forests inside its borders (see Figure 1). This is represented by differences in the spatial frequency of debris flow initiation (I_{DF}) and debris flow density (D_{DF}), which are recorded in Table 2 (page 20). Industrial forest I_{DF} is > 4 times greater than old-growth I_{DF}, whether calculated using all source areas or only those of high-confidence debris flow tracks. Primary D_{DF} is 1.8 times greater in the industrial forest than in the old-growth. D_{DF} calculated on the basis of cumulative runout length is 3.1 times higher in the industrial forest. Whether calculated on the basis of all mapped debris flows or only high confidence debris flows, D_{DF}* is approximately three times higher in the industrial forest than in the old growth.

Most creeks identified as debris flow tracks on the aerial photographs were not field checked, but of nine creeks in old-growth forest that were identified as debris flow tracks in the aerial photograph analysis and visited in the field, only four were found to have the characteristics of catastrophic debris flow disturbance (e.g., vegetation scoured from the channel and sideslopes, fresh deposits of poorly-sorted angular clasts jumbled up with woody debris, a terminal debris fan). The other five creeks lacked evidence of recent debris flow activity, and were misinterpreted as debris flow

tracks in the aerial-photograph survey due to their relatively open canopies and the presence of local side-slope failures along their lengths. All of the industrial forest channels that were visited in the field were proper debris flow tracks, and based on ridge-top visual reconnaissance I estimate that most (if not all) of the industrial forest channels identified as debris flow tracks on air photos have indeed experienced debris flow disturbance. Hence, I may have underestimated the differences between forest classes with respect to D_{DF} and I_{DF}, but I certainly have not overestimated it.

Although debris flow tracks are more common in the industrial forest than in the old-growth, individual debris flows do not appear to travel further along channels in the industrial forest. The distribution of primary runout lengths is similar for the industrial forest and old-growth areas (Figure 3, page 22), and although the distribution is shifted towards lower values for old-growth forest, the mean primary runout in the old growth is not significantly lower than that in the industrial forest (Table 2). In contrast, the difference in cumulative runout length distribution between the old-growth and industrial forests (Figure 4, page 22) reflects the greater proportion of the channel network affected by debris flows outside of the park. The mean cumulative runout in the industrial forest is almost twice that of the old growth, a difference that is highly significant (Table 2).

3.2. Field Survey

There are discrete deposits of sediment separated by stretches of bedrock channel

along the surveyed debris flow runout paths in both forest types, as shown by the sediment volume profiles (Figure 5, page 23). There are fewer sediment deposits in industrial forest debris flow tracks, however, and they tend to be of shorter length and lesser volume than those in old-growth channels. Where wood is present as a bed-forming material there can be large accumulations of sediment well upstream of the final deposition zone, a pattern that is particularly evident in the profiles of SP, HBC, WT, and HR5, all of which occur within old-growth stands. In both forest types sediment volume varies widely for reaches below 15% slope (Figure 6, page 24). Several of the low-gradient reaches plotted in Figure 5 are located at the downstream end of the debris flow tracks, where terminal deposition begins, but the differences between industrial and old-growth forests are most apparent in the zone of transport and partial deposition above 15% slopes. In the industrial forest reaches sediment volume declines with increasing gradient (log-log regression $R = -0.40$, $p = 0.007$) and is consistently below 250 $m^3/100$ m at slopes > 15%. In contrast, sediment volume in the old growth does not significantly correlate with reach slope (log-log regression $R = -0.26$, $p = 0.06$) and at slopes > 15% is higher than that of equally steep reaches in the industrial forest.

Debris flow runout zones in old-growth forest generally retain more sediment than those in industrial forest. Figure 7 (page 24) represents the distribution of channel sediment volumes for each forest class, excluding terminal deposition reaches. Over 90% of the industrial forest reaches have sediment volumes below the median

sediment volume of old-growth reaches. The geometric mean sediment volume for reaches in industrial forest is less than one tenth that of reaches in old-growth forest, and the total sediment volume per unit length for all channels is 7.7 times higher in old-growth forest (Table 3, page 21).

Debris flows in the industrial forest leave channels scoured to bedrock along much of their length, but in the old growth such scour is rare, and reaches tend to retain sediment cover along most of their length. Lower sediment volumes correspond to greater proportions of exposed bedrock in steeper reaches, although there is no unequivocal correlation between reach slope and bedrock exposure in either forest class (Figure 8, page 25). In the old-growth 60% of reaches can be classified as "alluvial" (< 25% bedrock exposure by length), 35% "transitional" (25% ≤ bedrock < 75%) and only 5% "bedrock" (≥ 75% bedrock exposure), whereas in the industrial forest only 14% of reaches are alluvial, 40% are transitional, and 46% are bedrock (Table 3).

Debris flows differ only slightly in their effect on channel margins in old-growth versus industrial forests in my study area. Sideslope scour (defined as the length of sideslopes without vegetative cover) is roughly equivalent between forest classes (Figure 9, page 25); the average proportion of scoured sideslopes for old-growth reaches is 41%, while for industrial forest reaches it is 53%. Approximately 20% of reaches in both forest classes have scoured sideslopes along 75% or more of their length. There is a higher proportion of reaches with less than 25% sideslope scour in

the old-growth, and a correspondingly lower proportion with between 25% and 75% scour, but the difference in means is only marginally significant ($p = 0.07$). Sideslope scour is weakly correlated with channel bedrock exposure (linear regression $R = 0.42$, $p = 0.0001$).

Most of the sediment retained along debris flow tracks in both forest types is stored in contiguous deposits directly upstream of concentrations of LWD (Figure 5). The huge wood and sediment deposit upstream of the 500 m mark in HR5 more than doubles the volume of sediment in the surveyed old-growth runout zone reaches. When data from HR5 are excluded from the analysis, 57% of old-growth sediment volume is directly associated with wood, 40% is in contiguous deposits upstream of concentrations of LWD, and only 3% is not associated with LWD at all. In industrial forest debris flow tracks 47% of old-growth sediment volume is directly associated with wood, 32% is in contiguous deposits upstream of concentrations of LWD, and 21% is not associated with LWD at all. Deposits in old-growth are typically larger than those in industrial-forest channels. Although LWD-free deposits are on average 1.5 times more voluminous in industrial-forest debris flow tracks, mixed sediment and wood deposits are between 5 and 13 times larger in old-growth channels (depending on whether or not HR5 is included in the analysis) and on average approximately 5 to 6 times as much sediment is stored in deposits upstream of LWD concentrations (Table 3).

There is more LWD in old-growth debris flow tracks, and it is directly involved in

the retention of substantial volumes of sediment. The difference in LWD load is reflected in the greater volume of mixed sediment-and-LWD deposits in the old-growth reaches. It is also reflected in my recording 1.8 times as many pieces of functioning LWD (LWD_F) per 100 m in old-growth channels as in industrial-forest channels. This difference is marginally significant ($p = 0.087$), but underestimates the true difference in LWD load because in many locations in the old-growth there were multiple pieces of LWD_F, and I only measured the key members.

In addition to the difference in amount of LWD_F, there are minor differences in its characteristics between forest types. The distributions of LWD_F diameter (Figure 10, page 26) have the same lower bounds in both forest classes, but there are larger diameter pieces in the old growth. There is, however, no significant difference in the geometric mean diameter between forest classes (Table 3). Most of the LWD that is functioning to retain sediment in both old-growth and industrial forests is of a diameter typical of old-growth forests and greater than can be expected to be recruited from industrial forests managed in short rotation [*Montgomery et al.*, 2003]. In both forest classes 50% of LWD_F is more than 60 cm in diameter, 75% over 40 cm, and 90% more than 30 cm in diameter. LWD_F pieces are significantly longer on average in the old-growth forest (Figure 11, page 26; Table 3). In addition, the maximum length of industrial-forest LWD_F is 15.5 m, while in the old-growth it is 40 m. There is no notable difference in the orientation of LWD_F with respect to the channel; the numbers of parallel and perpendicular pieces are about equal in both forest types.

TABLE 2. Landscape-Scale Debris Flow Parameters

	Industrial Forest	Old-growth Forest	t-test *p*-value
Landscape Characteristics			
Upland Area (km^2)	144	244	
Drainage Density (km/km^2)	3.02	2.79	
Debris Flow Density			
Primary D_{DF} (km/km^2)	0.55	0.30	
Cumulative D_{DF} (km/km^2)	1.37	0.44	
D_{DF}*	0.45	0.16	
High Confidence D_{DF}*	0.18	0.06	
Debris Flow Initiation			
I_{DF} ($no./km^2$)	3.89	0.82	
High Confidence I_{DF} ($no./km^2$)	1.06	0.24	
Primary Runout Distance			
Median R_P (km)	0.99	0.87	
Mean R_P (km)	1.11	1.02	0.49
Cumulative Runout Distance			
Median R_C (km)	2.16	1.08	
Mean R_C (km)	2.80	1.48	0.0001

D_{DF} Debris flow Density
D_{DF}* Dimensionless Debris flow Density
I_{DF} Debris flow Initiation
R_P Primary Runout Length
R_C Cumulative Runout Length

TABLE 3. Channel- and Reach-Scale Runout-Zone Parameters

	Industrial Forest	Old-growth Forest	t-test *p*-value
Channel Bed Character			
Mean Bedrock Proportion	63%	25%	< 0.0001
Alluvial Reaches	14%	60%	
Transitional Reaches	40%	35%	
Bedrock Reaches	46%	5%	
Sideslope Character			
Mean Scour Proportion	53%	41%	0.07
< 25% Scour	17%	37%	
25-75% Scour	63%	42%	
≥ 75% Scour	20%	5%	
Channel Sediment Volume (m^3/m):			
Total	0.78	6.02 (3.64)[a]	
Reach Geometric Mean	0.23	2.71 (2.44)[a]	< 0.0001
Average Deposit Volume (m^3/m):			
Directly Associated w/ LWD	0.51	6.54 (2.79)[a]	
Contiguous Upstream of LWD	0.34	1.56 (1.98)[a]	
Not Associated with LWD	0.22	0.13 (0.15)[a]	
Large Woody Debris			
Mean LWD_F/100 m	1.88	3.45	0.09
Geometric Mean LWD_F Length (m)	4.6	7.1	0.002
Geometric Mean LWD_F Diameter (cm)	55	60	> 0.3

a. Volumes in parentheses exclude HR5

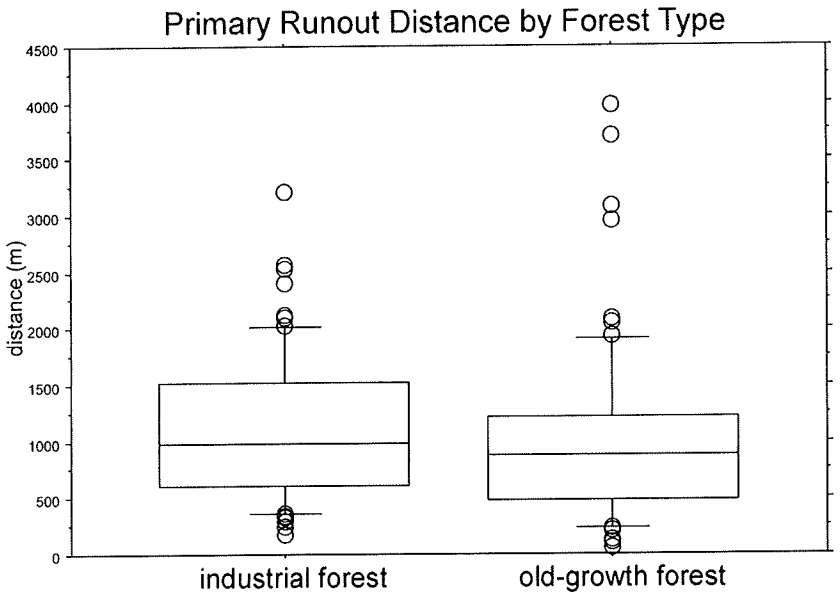

Figure 3: Primary Runout Distance Distributions. The middle line represents the median, the box spans the 25th to 75th percentiles, and the whiskers extend to the 10th and 90th percentiles. The median primary runout is 0.99 km for industrial forest (N = 68) and 0.87 km for old-growth (N = 68). The distributions are positively skewed; the mean primary runout is 1.11 km for industrial forest and 1.02 km for old-growth.

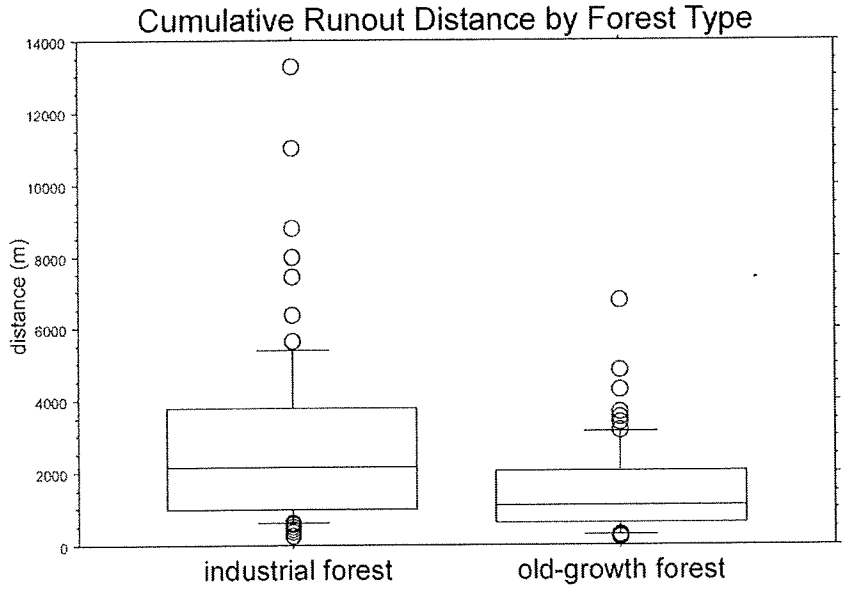

Figure 4: Cumulative Runout Distance Distributions. The middle line represents the median, the box spans the 25th to 75th percentiles and the whiskers extend to the 10th and 90th percentiles. The median cumulative runout is 2.16 km for industrial forest (N = 68) and 1.08 km for old-growth (N = 68). The distributions are positively skewed; the mean cumulative runout is 2.80 km for industrial forest and 1.48 km for old-growth.

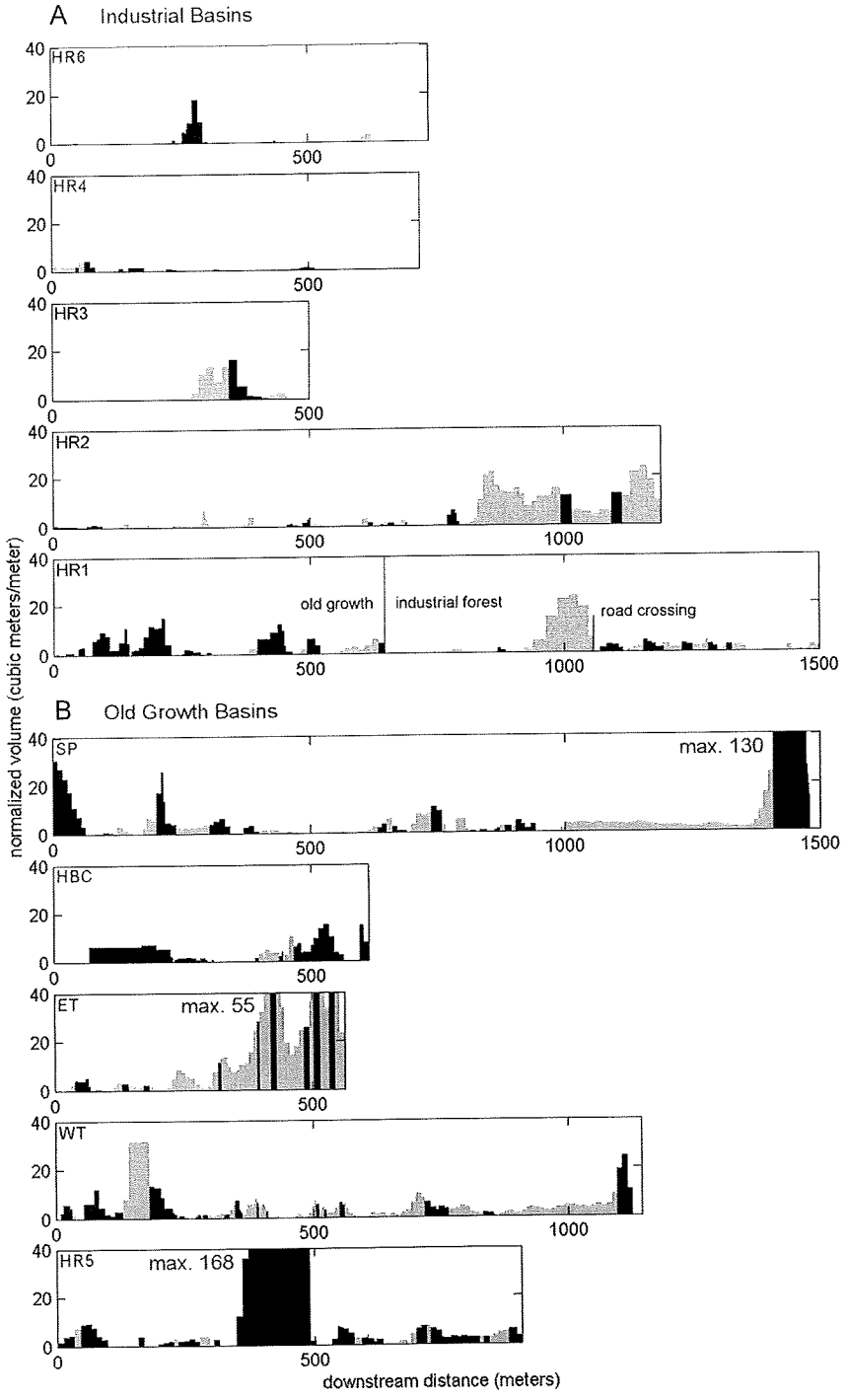

Figure 5: Sediment volume profiles. Black areas represent mixed sediment and LWD deposits, grey areas represent sediment only. Sediment volumes are normalized by length, so area in the figure is proportional to volume in the field. A: Industrial forest channels and HR1, which travels through old-growth forest in its upper reaches and industrial forest downstream of 650 m. B: Old-growth channels.

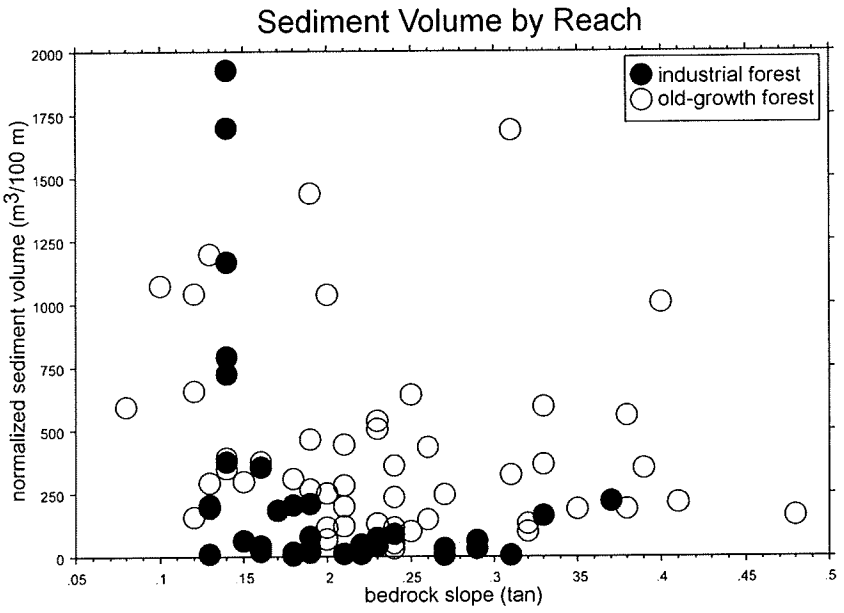

Figure 6: Sediment volume versus reach average (bedrock) gradient. The diameter of the markers represents the estimated uncertainty in slope, see text for discussion of uncertainty in estimated sediment volume.

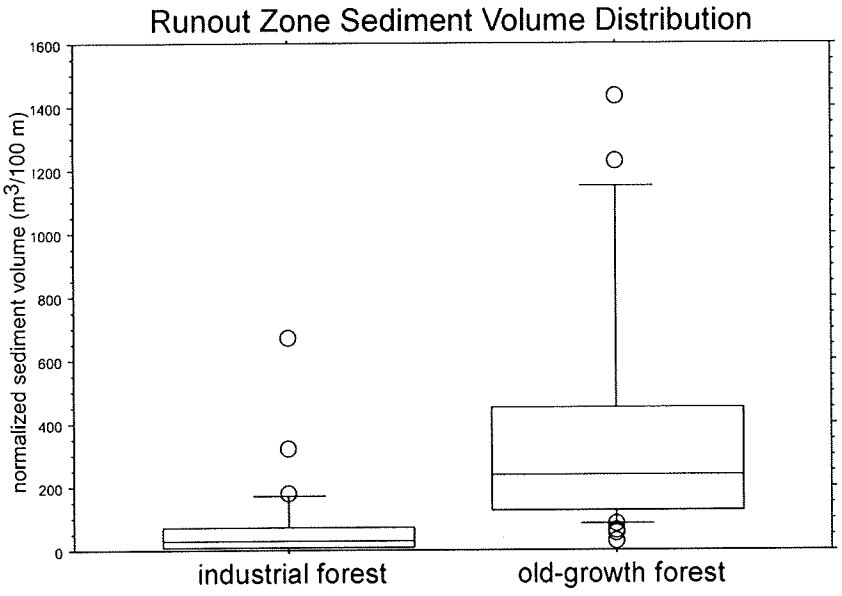

Figure 7: Sediment Volume Distributions. The middle line represents the median, the box spans the 25th to 75th percentiles and the whiskers extend to the 10th and 90th percentiles. The median sediment volume is 28 m^3/100 m for industrial forest (N = 35) and 239 m^3/100 m for old-growth (N = 43). The distributions are positively skewed; the mean sediment volume is 75 m^3/100 m for industrial forest and 606 m^3/100 m for old-growth.

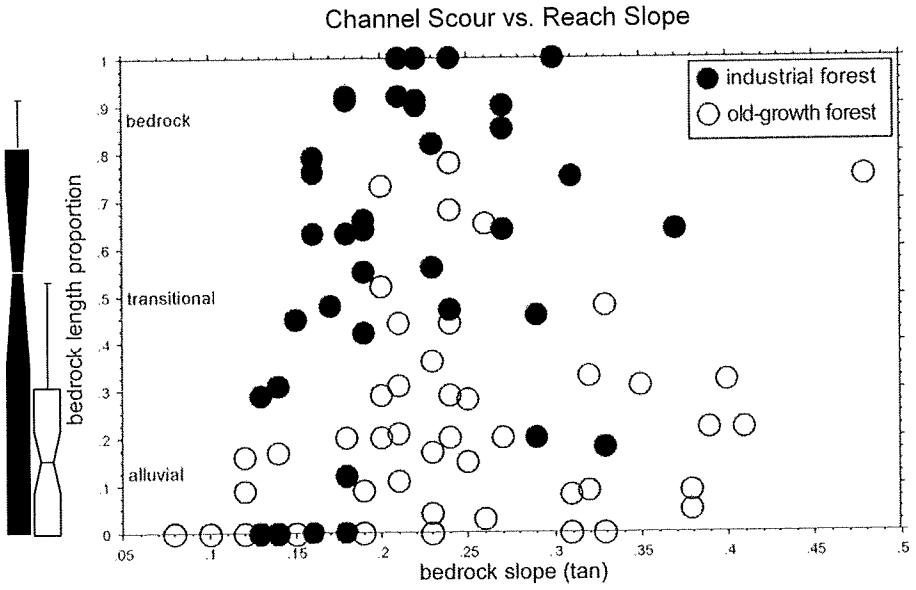

Figure 8: Channel bedrock proportion versus reach average (bedrock) gradient. The diameter of the markers approximately represents the estimated uncertainty in slope and bedrock proportion. In the box plots to the left of the figure the middle line represents the median, the notch represents the 95% confidence interval for the median, the box spans the 25th to 75th percentiles and the whiskers extend to the 10th and 90th percentiles.

Figure 9: Scoured sideslope proportion versus reach average (bedrock) gradient. The diameter of the markers approximately represents the estimated uncertainty in slope. In the box plots to the left of the figure the middle line represents the median, the notch represents the 95% confidence interval for the median, the box spans the 25th to 75th percentiles and the whiskers extend to the 10th and 90th percentiles.

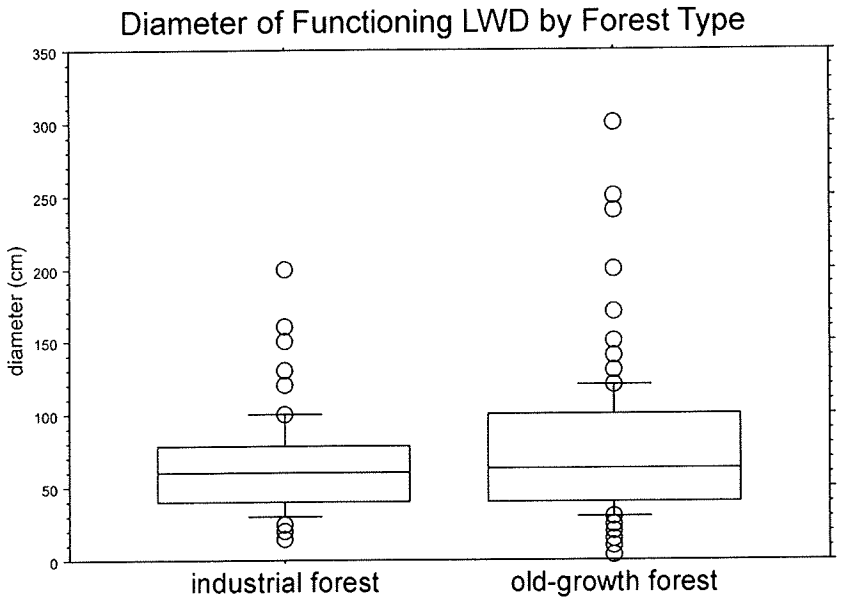

Figure 10: LWD_F Diameter Distributions. The middle line represents the median, the box spans the 25th to 75th percentile and the whiskers extend to the 10th and 90th percentiles. The median LWD_F diameter is 60 cm for both industrial (N = 79) and old-growth forest (N = 179). The distributions are slightly positively skewed; the mean LWD_F diameter is 63 cm for industrial forest and 72 cm for old-growth.

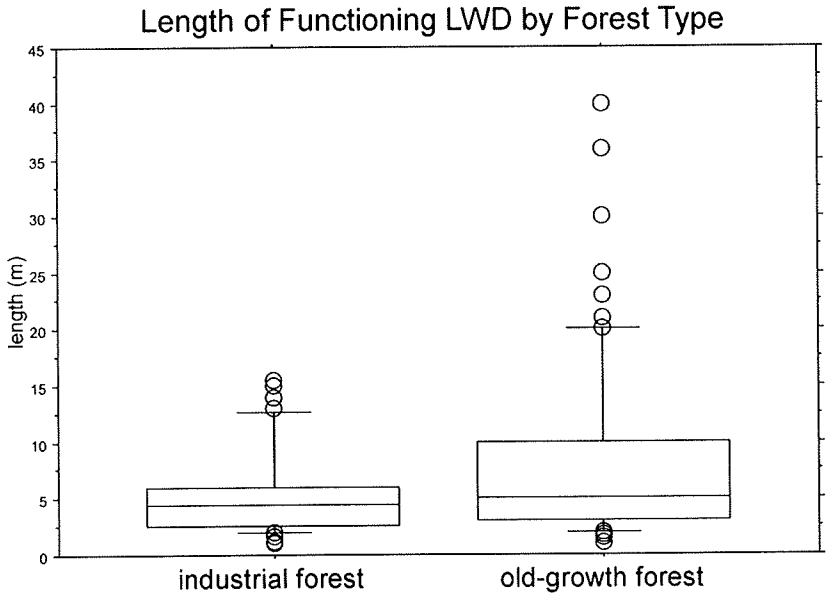

Figure 11: LWD_F Length Distributions. The middle line represents the median, the box spans the 25th to 75th percentile and the whiskers extend to the 10th and 90th percentiles. The median length of LWD_F is 5.0 m for industrial (N = 48) and 6.3 m for old-growth forest (N = 127). The distributions are positively skewed; mean LWD_F length is 5.7 m for industrial forest and 10.4 m for old-growth.

4. DISCUSSION

4.1. Landscape scale

My observation that mean primary runout length (R_P) is equivalent between forest types contrasts with the results of *May* [1998], who found that runout distance tends to be greater for debris flows that originate in or travel through clear-cut industrial forest. Like *May* [1998], however, I did find greater average cumulative (R_C) runout resulting from the greater number of source areas per basin in industrial forests. The difference in findings stems at least in part from the difference in drainage network structure. In a dendritic network such as that of May's [1998] Oregon Coast Range (OCR) study area there are many opportunities for debris flows to stop at channel intersections, and indeed *Benda and Cundy* [1990] found that they could predict terminal deposition based on a threshold intersection angle of 70°. In pinnate drainage networks such as that of the western Olympic Mountains such high-angle tributary junctions are rare and primary runout lengths are largely determined by the distances between failure-prone headwater hollows and the intersection of low-order channels with unconfined, low gradient mainstem valleys. This distance is a function of drainage basin geometry, and in my study area does not substantially differ between the industrial and old-growth basins.

While I did not attempt to inventory all landslides, I did find that debris flow inducing landslides are more common in the industrial forests in my study area, as

represented by over four times higher I_{DF} and approximately three times higher cumulative D_{DF}. Although landslides under old-growth canopy may be undercounted in some aerial-photograph-based inventories [*Pyles and Froehlich*, 1987; and see *Robison et al.*, 1999 for an extensive discussion], I found that I *over-counted* debris flows in the old-growth due to my method of inferring the presence of debris flow tracks from canopy openings along headwater channels. Because I surveyed at only one point in time, I cannot directly address frequency, but the fact that debris flow scars are more common in the industrial forests suggests that debris-flow-inducing landslides are more frequent.

Many authors have observed that the rate of landsliding increases after clear-cutting [e.g., *Johnson et al.*, 2000; *Snyder*, 2000; *May*, 2002]. Slope-stability analysis can be used to explain this increase as a consequence of decreased soil cohesion following timber harvest, and to predict the depth of soil loss that can be expected to result from this effect. One of the most widely used slope stability models is the infinite-slope model [*Selby*, 1993], in which

$$FS = \frac{\left[C + \left(\rho_S - m\rho_W\right) gD \cos\theta \tan\phi\right]}{\left(\rho_S gD \sin\theta\right)} \tag{2}$$

where FS is the factor of safety, C is cohesion, ρ_S is the density of soil, ρ_W the density of water, m is the saturated fraction of the depth to the failure plane, g the acceleration due to gravity, D the slope-normal depth to the failure plane, θ is the slope of the surface (and failure plane), and ϕ the internal friction angle of the

material. Rearranging (2) to solve for soil depth at $FS = 1$, results in

$$D = \frac{C}{\rho_S g \left(\sin\theta - \cos\theta \tan\phi\right) + m\rho_W g \cos\theta \tan\phi}. \quad (3)$$

Using (3) it is possible to predict the maximum depth of stable soil for a given combination of slope, soil density, cohesion, friction angle, and saturation. For my calculations I used ρ_S = 2000 kg m^{-3}, ρ_W = 1000 kg m^{-3}, ϕ = 35° and m = 0.5, representing partial saturation of the soil mantle. In Figure 12 (page 34) I plot the maximum depth of stable soil against slope for cohesion of 10 and 2 kPa to span the expected range between minimum cohesion for old-growth and recently clear-cut forests respectively [e.g., *Schaub*, 1999; *Montgomery et al.*, 2000; *Schmidt et al.*, 2001]. The expected change in the maximum depth of stable soil between old-growth and clear-cut hillslopes, assuming sufficient time to achieve equilibrium, is between 1.5 and 0.7 m for slopes between 40° and 60°. Landsliding should be more common in episodically or periodically clear-cut forests, because soil mantle thickness is out of equilibrium during post-harvest periods of low cohesion (Figure 13, page 34).

Landsliding in the clear-cut portion of my study area occurred both in hillslope hollows and on planar hillsides [e.g., *Logan et al.*, 1991]. This is also to be expected, because soil production declines with soil depth and becomes negligible at about 1 m [*Heimsath et al.*, 1997, 1999], which is shallower than the maximum stable depth for slopes < 48° under old-growth forest (see Figure 10). Hence, under an old growth forest with high cohesion, the soil on planar and divergent slopes will not tend to

become deep enough to fail, while on convergent slopes (i.e., hollows) soils will tend to increase in depth due to creep until they exceed the stable depth and eventually fail [*Dietrich and Dunne*, 1978; *Dietrich et al.*, 1995]. Only once the cohesion of the soil has been reduced after timber harvest would one expect to see widespread failure on planar and divergent slopes [*Montgomery et al.*, 1998]. Although it is generally thought that protecting headwater hollows from disturbance is sufficient to reduce the potential for slope failure [*Schlichte*, 1991], this result suggests that steep planar slopes are particularly vulnerable to failure after clear-cut timber harvesting. It also suggests that hillslopes that are subject to clear-cut timber harvest will contribute more sediment to the channel system than those left in old-growth forest, as reported by many authors [e.g., *Roberts and Church*, 1986; *Logan et al.*, 1991; *Montgomery et al.*, 2000; *Guthrie*, 2002].

4.2. Channel scale

Based in part on the results of their landscape evolution model *Lancaster et al.* [2001] argue that where debris flows are common and wood is plentiful, large volumes of sediment can be stored high in drainage networks. In both industrial and old-growth forest in my study area most of the sediment volume in debris flow impacted headwater channels is directly or indirectly stored by LWD. Mixed wood and sediment deposits are typically five to thirteen times larger in old-growth debris flow tracks and there are on average at least 1.8 times as many pieces/100 m of

sediment-retaining LWD. Not surprisingly, there is five (averaged by channel) to eleven (averaged by reach) times as much sediment in old-growth as there is in industrial-forest debris flow runout zones. I found sediment volumes on the order of those reported by *Lancaster et al.* [2001] in four out of five (HR5, HR1, HBC, SP) of the old-growth channels I surveyed. Because they have low surface gradients and small drainage areas, these deposits are unlikely to be rapidly dispersed by fluvial processes [*Perkins*, 1989; *O'Connor*, 1994].

There are multiple deposits in each channel where sediment was retained upstream of LWD concentrations. It is unclear whether these concentrations of LWD and sediment reflect pre-existing log jams that stopped part of a debris flow, or dynamic snout deposition during the debris flow itself, as described by *Parsons et al.* [2001] for experimental debris flows and inferred by *Whipple* [1994] for debris flows lacking LWD. In any case, I found that most reaches along debris flow tracks in wood-rich old-growth forest channels retain sediment and that bare bedrock is relatively rare. This observation contrasts with the results of *May* [2001] for the Oregon Coast Range and the widespread assertion that debris flows scour headwater streams to bedrock, but I did find extensive bedrock exposure in the relatively wood-depleted industrial forest channels.

May [2001] found an increase in channel sediment volume over time following debris flow disturbance in mature forest of the Oregon Coast Range, with negligible sediment volume in present in the first 30 years. The channels in my study have all

experienced debris flows within the past 30 years, but only those in the industrial forest have sediment volumes similar to those of recent debris flow tracks in May's study (Figure 14, page 35). The steeper old-growth reaches in this study have sediment volumes comparable to those that *May* [2001] found in channels that had not experienced a debris flow in over 100 years. Whether this reflects greater sediment retention during debris flows or a higher post-debris-flow sediment input rate is not clear, and cannot be resolved with the data from this study alone. It is also unclear whether channel sediment volume increases over time in this area as it is thought to in the Oregon Coast Range. To resolve such questions it will be necessary to collect additional sediment volume data from western Olympic headwater channels across a range of disturbance ages.

4.3. Synthesis

I suggest that the differences in both debris flow frequency and channel sediment storage between old-growth and industrial forests represent a fundamental shift in the sediment production and transport system (Figure 15, page 33), akin to that suggested by *Gabet and Dunne* [2002] for California grasslands. Under old-growth forest, short-term excess sediment delivered to the channel network can be stored in LWD-rich headwater channels, so sediment supply to higher order streams is buffered from the stochastic inputs of mass wasting. Overall sediment production is low (due to the thickness of the soil mantle), sediment storage in the channels is high, and sediment

output from headwater streams is low. When forests are clear-cut and the effective cohesion of the soil declines, the equilibrium hillslope soil thickness decreases and planar and divergent slopes (as well as hollows) become prone to instability, resulting in an accelerated rate of landsliding. The sediment delivered to the streams by mass-wasting episodes is not retained in steep headwater reaches due to a lack of LWD-mediated storage capacity, and is instead delivered *en masse* to lower gradient reaches by debris flows. This state of low sediment production and high sediment output is necessarily transient, and can only last until the hillslopes have shed their excess sediment, at which point sediment production will be higher due to thinner soils, channels will have little storage capacity (assuming a continued dearth of old-growth class LWD), and sediment flux from the hillslopes will be rapidly transmitted through headwater streams to the rest of the drainage network.

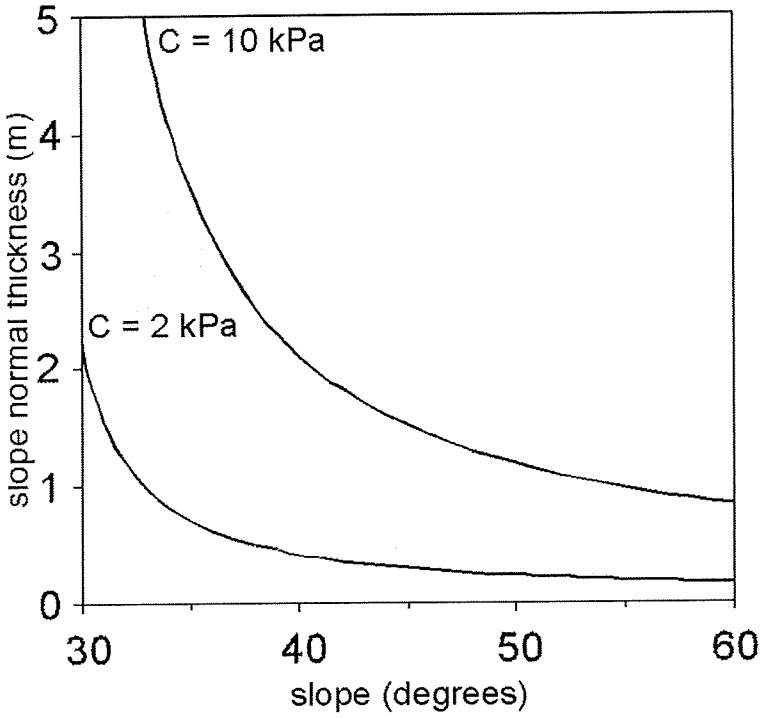

Figure 12: Predicted Maximum Stable Soil Thickness Versus Slope. Plotted curves are representative of hillslopes in old-growth (C = 10 kPa) and clear-cut (C = 2 kPa) forests that fail at partial saturation (m = 0.5). The shaded area between the curves represents the change in equilibrium soil thickness expected to result from clear-cut timber harvest.

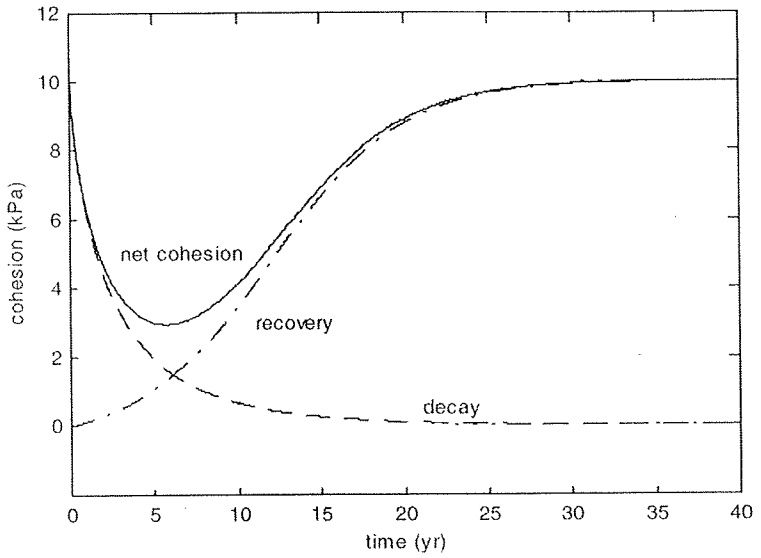

Figure 13: Decline in Soil Cohesion Following Disturbance. Adapted from *Schaub* [1999].

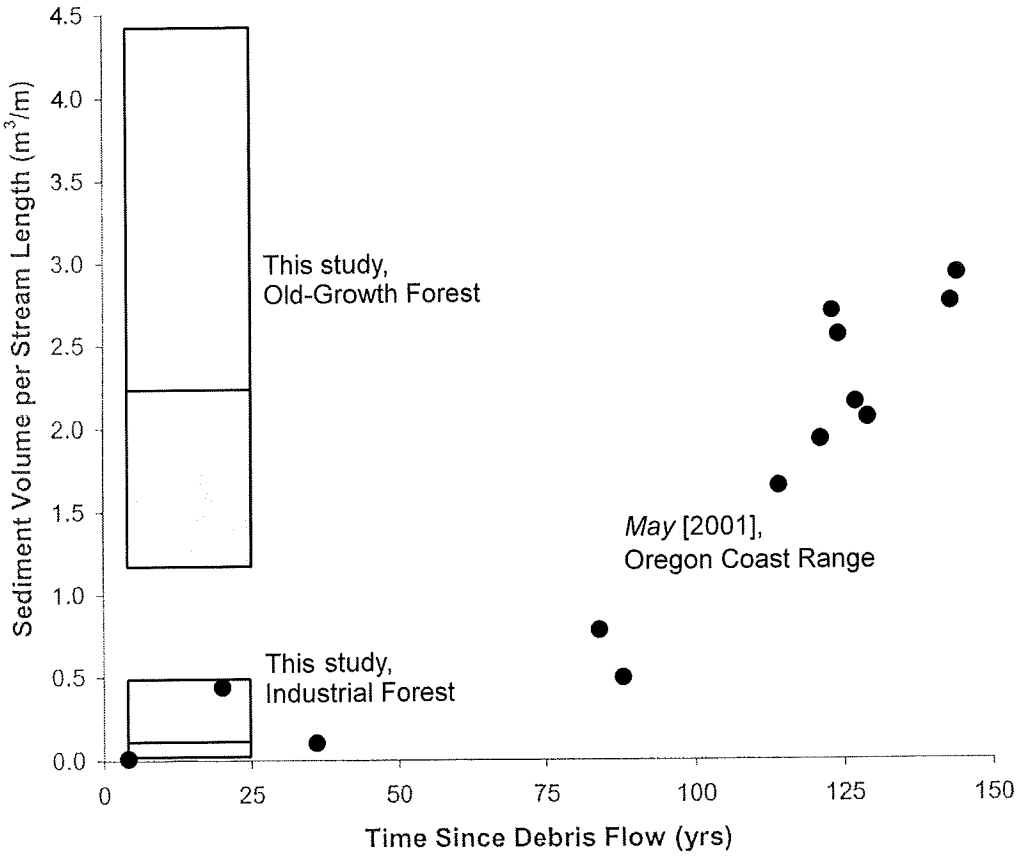

Figure 14: Post-Debris-Flow Sediment Volume vs. Time. Adapted from *May* [2001]. Filled circles represent May's data for channels in the Oregon Coast Range with gradients > 0.2. Boxes represent sediment volumes for reaches in this study with bedrock gradients > 0.2; the middle line represents the median, and the box spans the 25th to 75th percentiles. The width of the boxes corresponds to the range of time since last debris flow (see Table 1).

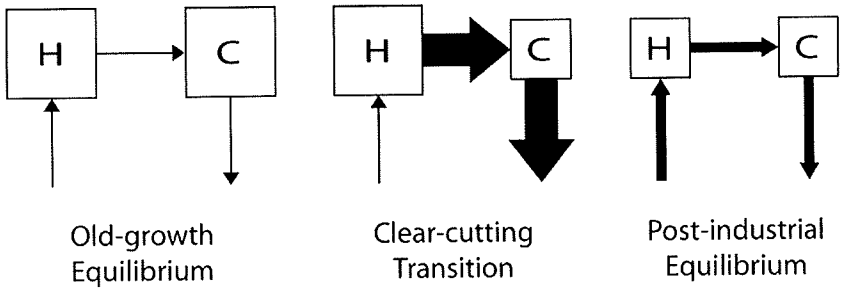

Figure 15: Conceptual model. The boxes represent storage on hillslopes (H) and in headwater channels (C). The up arrows represent weathering flux, the right arrows mass-wasting, and the down arrows debris flow and fluvial transport out of the headwater channels. The relative size of the elements represents the relative magnitudes of stores and fluxes.

5. SUMMARY AND CONCLUSIONS

Old-growth and industrial forests in the western Olympic Mountains differ significantly in debris flow density and occurrence; debris flow initiation sites are more than four times as common and debris flow density is three times higher in the industrial forest. Although primary runout lengths are similar, old-growth and industrial forests also differ in mean cumulative runout length and in the amount of sediment and wood remaining in headwater channels in the wake of debris flow disturbance; cumulative runout is three times higher and sediment and wood volumes are 5 to 10 times lower in the industrial forest. The difference in sediment retention leads to a greater proportion of exposed bedrock channel in industrial forest areas: 46% of surveyed reaches were predominantly bedrock-floored in industrial forests, compared to 5% in old-growth forests. These differences are most pronounced in reaches above 15% slope. The bulk of the sediment on the bed of debris flow impacted channels is retained in contiguous deposits upstream of concentrations of LWD. There is less LWD in the industrial channels and correspondingly less sediment stored along the debris flow path. Most of the functional LWD in both forest types is of a diameter greater than will be provided by forests managed for timber in clear-cut rotation.

Industrial forestry has a profound influence on sediment transport by mass movement in the western Olympics. Forest clearing both increases the frequency and

changes the effect of debris flows, resulting in fundamentally different hillslope and channel sediment storage and reach morphology in industrial forests and old-growth forests. Sustained short-rotation harvest of forest from the hillsides of headwater basins and removal of old-growth LWD from headwater channels can be expected to lead eventually to a stable state in which soil depth on hillslopes and sediment storage in headwater channels is relatively low, and sediment output to higher order reaches is dependent on and tightly coupled to the rate of sediment production on the hillslopes. During the transition from old-growth to industrial forest sediment storage on hillslopes is diminishing, sediment storage in channels is low, and sediment output from headwater channels is high.

LIST OF REFERENCES

Abbe, T.B. and D.R. Montgomery, 1996, Large woody debris jams, channel hydraulics, and habitat formation in large rivers, *Regulated Rivers: Research and Management, 12*, 201-221.

Abbe, T.B. and D.R. Montgomery, 2003, Patterns and processes of wood debris accumulation in the Queets River basin, Washington, *Geomorphology, 51*, 81-107.

Benda, L.E., 1988, Debris flows in the Tyee formation of the Oregon Coast Range, M.S. thesis, Univ. of Washington, Seattle.

Benda, L.E., 1990, The influence of debris flows on channels and valley floors in the Oregon Coast Range, U.S.A., *Earth Surface Processes and Landforms, 15,* 457-466.

Benda, L.E., and T.W. Cundy, 1990, Predicting deposition of debris flows in mountain channels, *Canadian Geotechnical Journal*, 27, 409-417.

Bilby, R.E., and J.W. Ward, 1991, Characteristics and function of large woody debris in streams draining old-growth, clear-cut, and second-growth forests in southwestern Washington, *Canadian Journal of Fisheries and Aquatic Science, 48,* 2499-2508.

Bugosh, N., and S.G. Custer, 1989, The Effect of a Log-Jam Burst on Bedload Transport and Channel Characteristics in a Headwaters Stream, in *Proceedings of the Symposium on Headwaters Hydrology*, edited by W.W. Woessner and D.F. Potts, pp. 203-211, American Water Resources Association, Bethesda.

Church, M., 2002, Geomorphic thresholds in riverine landscapes, *Freshwater Biology, 47*, 541-557.

Dieterich, M., and N.H. Anderson, 1998, Dynamics of abiotic parameters, solute removal and sediment retention in summery-dry headwater streams of western Oregon, *Hydrobiologia, 379,* 1-15.

Dietrich, W.E., and T. Dunne, 1978, Sediment budget for a small catchment in mountainous terrain, *Zeitschrift für Geomorphologie, Supplementbund 29,* 191-206.

Dietrich, W.E., R. Reiss, M.L. Hsu, and D.R. Montgomery, 1995, A process-based model for colluvial soil depth and shallow landsliding using digital elevation data, *Hydrological Processes, 9,* 383-400.

Edmonds, R.L., 1998, *Vegetation patterns, hydrology, and water chemistry in small watersheds in the Hoh River Valley, Olympic National Park*, U.S. Dept. of the Interior, National Park Service, Denver.

Fetherston, K.L., R.J. Naiman, and R.E. Bilby, 1995, Large woody debris, physical process, and riparian forest development in montane river networks of the Pacific Northwest, *Geomorphology, 13*, 133-144.

Ford, E.D., 2000, *Scientific Method for Ecological Research*, Cambridge University Press, Cambridge.

Froehlich, H.A., 1973, Natural and man-caused slash in headwater streams, *Oregon Logging Handbook 33*, Pacific Logging Congress.

Gabet, E.J., and T. Dunne, 2002, Landslides on coastal sage-scrub and grassland hillslopes in a severe El Niño winter: The effects of vegetation conversion on sediment delivery, *Geological Society of America Bulletin, 114(8)*, 983-990.

Gomi, T., R.C. Sidle, and J.S. Richardson, 2002, Understanding processes and downstream linkages of headwater systems, *Bioscience, 52(10)*, 905-916.

Gomi, T., R.C. Sidle, M.D. Bryant, and R.D. Woodsmith, 2001, The characteristics of woody debris and sediment distribution in headwater streams, southeastern Alaska, *Canadian Journal of Forest Research, 31*, 1386-1399.

Guthrie, R.H., 2002, The effects of logging on frequency and distribution of landslides in three watersheds on Vancouver Island, British Columbia, *Geomorphology, 43,* 273-292.

Heimsath, A.M., W.E. Dietrich, K. Nishiizumi, and R.C. Finkel, 1997, The soil production function and landscape equilibrium, *Nature, 388,* 358-361.

Heimsath, A.M., W.E. Dietrich, K. Nishiizumi, and R.C. Finkel, 1999, Cosmogenic nuclides, topography, and the spatial variation of soil depth, *Geomorphology, 27,* 151-172.

Heusser, C.J., 1974, Quaternary vegetation, climate, and glaciation of the Hoh River Valley, Washington, *Geological Society of America Bulletin, 85*, 1547-1560.

Johnson, A.C., D.N. Swanston, and K.E. McGee, 2000, Landslide initiation, runout, and deposition within clearcuts and old-growth forests of Alaska, *Journal of the American Water Resources Association, 36(1)*, 1097-1113.

Lancaster S.J., S.K. Hayes and G.E. Grant, 2001, Modeling sediment and wood storage and dynamics in small mountainous watersheds, pp. 85-102 in *Geomorphic Processes and Riverine Habitat*, edited by J.M. Dorava, D.R. Montgomery, B.B. Palcsak, & F.A. Fitzpatrick, American Geophysical Union, Washington, DC.

Logan, R.L., K.L. Kaler, and P.K. Bigelow, 1991, Prediction of sediment yield from tributary basins along Huelsdonk Ridge, Hoh river, Washington, *Washington Division of Geology and Earth Resources Open File Report 91-7*, Washington State Department of Natural Resources, Olympia.

May, C.L., 1998, *Debris Flow Characteristics Associated with Forest Practices in the Central Oregon Coast Range*, M.S. thesis, Oregon State Univ., Corvallis.

May, C.L., 2001, *Spatial and Temporal Dynamics of Sediment and Wood in Headwater Streams in the Central Oregon Coast Range*, Ph.D. thesis, Oregon State Univ., Corvallis.

May, C.L., 2002, Debris flows through different forest age classes in the central Oregon Coast Range, *Journal of the American Water Resources Association, 38,* 1097-1113.

McHenry, M.L., E. Shott, R.H. Conrad, and G.B. Grette, 1998, Changes in the quantity and characteristics of large woody debris in streams of the Olympic Peninsula, Washington, U.S.A. (1982-1993), *Canadian Journal of Fisheries and Aquatic Sciences., 55*, 1395-1407.

Montgomery, D.R., and J.M. Buffington, 1998, Channel Processes, Classification, and Response, in *River Ecology and Management: Lessons from the Pacific Coastal Ecoregion*, edited by R.J. Naiman and R.E. Bilby, pp. 13-42, Springer-Verlag, New York.

Montgomery, D.R., J.M. Buffington, R.D. Smith, K.M. Schmidt, and G. Pess, 1995, Pool spacing in forest channels, *Water Resources Research, 33(4)*, 1097-1105.

Montgomery, D.R., K. Sullivan, and H.M. Greenberg, 1998, Regional test of a model for shallow landsliding, *Hydrological Processes, 12,* 943-955.

Montgomery, D.R., K.M. Schmidt, H.M. Greenberg, and W.E. Dietrich, 2000, Forest clearing and regional landsliding, *Geology, 28(4),* 311-314.

Montgomery, D.R., T.B. Abbe, J.M. Buffington, N.P. Peterson, K.M. Schmidt, and J.D. Stock, 1996, Distribution of bedrock and alluvial channels in forested mountain drainage basins, *Nature, 318*, 587-589.

Montgomery, D.R., T.M. Massong, and S.C.S. Hawley, 2003, Influence of debris flows and log jams on the location of pools and alluvial channel reaches, Oregon Coast Range, *Geological Society of America Bulletin, 115(1)*, 78-88.

Morrison, P.H., 1975, Ecology and Geomorphological Consequences of Mass Movements in the Alder Creek Watershed and Implications for Forest Land Management, B.A. thesis, University of Oregon, Eugene.

Murphy, M.L., and K.V. Koski, 1989, Input and depletion of woody debris in Alaska streams and implications for streamside management, *North American Journal of Fisheries Management, 9*, 423-436.

O'Connor, M.D., 1994, *Sediment Transport in Steep Tributary Streams and the Influence of Large Organic Debris*, Ph.D. Thesis, Univ. of Washington.

Parsons, J.D., K.X. Whipple, and A. Simoni, 2001, Experimental Study of the Grain-Flow, Fluid-Mud Transition in Debris Flows, *Journal of Geology, 109*, 427-447.

Perkins, S.J., 1989, Landslide deposits in low-order streams – their erosion rates and effects on channel morphology, in *Proceedings of the Symposium on Headwaters Hydrology*, edited by W.W. Woessner and D.F. Potts, pp. 173-182, American Water Resources Association, Bethesda.

Peterson, D.L., E.G. Schreiner, and N.M. Buckingham, 1997, Gradients, Vegetation and Climate: Spatial and Temporal Dynamics in the Olympic Mountains, U.S.A., *Global Ecology and Biogeography Letters, 6(1)*, 7-17.

Pyles, M.R., and H.A. Froehlich, 1987, Rates of Landsliding as Impacted by Timber Management Activities in Northwestern California, *Bulletin of the Association of Engineering Geologists, 24, (3)*, 425-431.

Ralph, S.C., G.C. Poole, L.L. Conquest, and R.J. Naiman, 1994, Stream channel morphology and woody debris in logging and unlogging basins of western Washington, *Canadian Journal of Fisheries and Aquatic Science*, *51*, 37-51.

Reneau, S.L., and W.E. Dietrich, 1991, Erosion rates in the southern Oregon Coast Range: evidence for an equilibrium between hillslope erosion and sediment yield, *Earth Surface Processes and Landforms, 16*, 307-322.

Roberts, R.G., and M. Church, 1986, The sediment budget in severely disturbed watersheds, Queen Charlotte Ranges, British Columbia, *Canadian Journal of Forest Research, 16*, 1092-1106.

Robison, E.G., K. Mills, J. Paul, L. Dent, and A. Skaugset, 1999, Storm impacts and landslides of 1996: final report, *Forest Practices Technical Report No. 4*, Oregon Department of Forestry.

Schaub, T.S., 1999, *Incorporating root strength estimates into a landscape-scale slope stability model through forest stand age inversion from remotely sensed data*, M.S. thesis, Univ. of Washington, Seattle.

Schlichte, K., 1991, Aerial photo interpretation of the failure history of the Huelsdonk Ridge/Hoh River area, unpublished report, Washington State Department of Natural Resources.

Schmidt, K.M., J.J. Roering, J.D. Stock, W.E. Dietrich, D.R. Montgomery and T.S. Schaub, 2001, Root cohesion variability and shallow landslide susceptibility in the Oregon Coast Range. *Canadian Geotechnical Journal, 38*, 995-1024.

Seidl, M.A., and W.E. Dietrich, 1992, The problem of channel erosion into bedrock, in *Functional Geomorphology, Catena Supplement 23*, 101-124.

Selby, M.J., 1993, *Hillslope materials and processes*, Oxford University Press, Oxford.

Shreve, R.L., 1969, Stream lengths and basin areas in topologically random channel networks, *Journal of Geology, 77(4)*, 397-414.

Sidle, R.C., Y. Tsuboyama, S. Noguchi, I. Hosoda, M. Fujieda, and T. Shimizu, 2000, Streamflow generation in steep headwaters: A linked hydro-geomorphic paradigm, *Hydrological Processes, 14,* 369-385.

Snyder, K.U., 2000, Debris Flows and Flood Disturbance in Small Mountain Watersheds, M.S. thesis, Oregon State Univ., Corvallis.

Swanson, F.J., and D.N. Swanston, 1977, Complex mass-movement terrains in the western Cascade Range, Oregon, *Reviews in Engineering Geology 3; Landslides,* 113-124.

Tabor, R.W., and Cady, W.M., 1978, Geologic map of the Olympic Peninsula, *U.S. Geological Survey Miscellaneous Investigations Series Map, I-993.*

Whipple, K.X., 1994, *Debris flow fans: process and form*, Ph.D. thesis, Univ. of Washington, Seattle.

Wohl, E., 2000, *Mountain Rivers*, Water Resources Monograph 14, American Geophysical Union, Washington D.C.

APPENDIX A: Channel profile calculation

To reduce the frequency of back sighting when surveying steep channels one can use an Abney level rather than an engineer's level or a hand level. Because the tape follows the ground surface and the readings from the stadia rod refer to the distance from a sloping line of unknown length projected from the Abney level (see Figure A.1, page 46), converting the recorded readings to an accurate profile requires different calculations than are used with a horizontal datum. Here I derive the necessary formulae.

In the field one records the sighting angle α, the distance along the ground surface between stations ΔS, and the stadia rod readings Z_0 and Z_1. From these one can calculate the horizontal distance between stations ΔL, the change in surface elevation ΔZ, and the surface slope β through the intermediate step of calculating the length of the sighting line ΔR as follows:

From Figure A.1,

$$\text{Angle } \Delta R \cdot \delta Z = 90° + \alpha,$$

so by the Law of Cosines

$$\Delta S^2 = \Delta R^2 + \delta Z^2 - 2\, \Delta R\, \delta Z \cos (90° + \alpha),$$

and rearranging gives

$$\Delta R^2 - [2\, \delta Z \cos (90° + \alpha)]\, \Delta R + (\delta Z^2 - \Delta S^2) = 0.$$

Applying the quadratic formula results in

$$\Delta R = \frac{2\delta Z \cos(90° + \alpha) \pm \sqrt{(2\delta Z \cos(90° + \alpha))^2 - 4(\delta Z^2 - \Delta S^2)}}{2},$$

which simplifies to

$$\Delta R = -\delta Z \sin\alpha + \sqrt{\delta Z^2 \sin^2\alpha - \delta Z^2 + \Delta S^2}\ .$$

The remaining parameters are determined by definition:

$$\Delta L = \Delta R \cos\alpha,$$

$$\Delta Z = \Delta R \sin\alpha + \delta Z,$$

$$\beta = \text{atan}\ (\Delta Z/\Delta L).$$

The same formulae apply where $Z_0 > Z_1$ or $\beta < 0$.

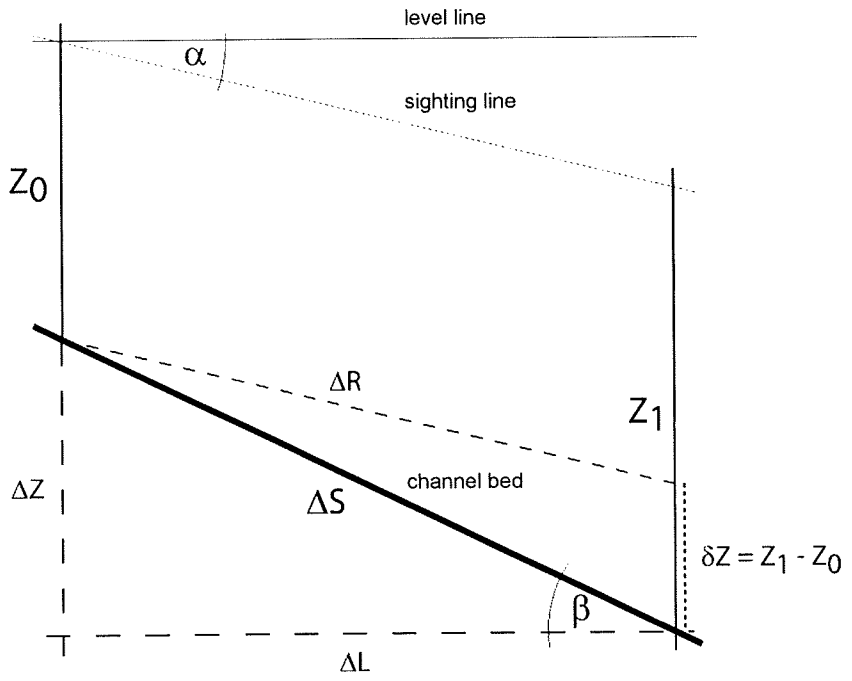

Figure A.1: Abstracted channel profile geometry. Field measurements are α, ΔS, Z_0 and Z_1. Derived measurements are ΔR, ΔL = ΔR cos α, ΔZ = ΔR sin α + δZ, and β = atan (ΔZ/ΔL).

APPENDIX B: Sediment volume calculations

Channel sediment volume formula derivation.

For channels with a roughly parabolic cross-section (Figure B.1, page 48) the cross-sectional area $A \approx \frac{2}{3}WD$, where W is the measured bed width and D the measured (or estimated) depth to bedrock. Using the method of infinitesimal slices to construct a channel segment of length L between measurements W_0, D_0 and W_1, D_1,

$$V = \int dV = \int A(\lambda)\, d\lambda,$$

where $d\lambda$ is the infinitesimal length of each slice. For each slice i,

$$A_i = \tfrac{2}{3} W_i D_i,$$

and assuming linear change in width and depth along the segment

$$W_i = W_0 + \lambda (W_1 - W_0)/L,$$

$$D_i = D_0 + \lambda (D_1 - D_0)/L.$$

For ease of calculation define

$$K_w = \Delta W/L = (W_1 - W_0)/L,$$

$$K_d = \Delta D/L = (D_1 - D_0)/L.$$

Substituting,

$$A_i = \tfrac{2}{3} (W_0 + \lambda K_w) (D_0 + \lambda K_d)$$

and rearranging,

$$A_i = \tfrac{2}{3} (K_w K_d \lambda^2 + K_w D_0 \lambda + K_d W_0 \lambda + W_0 D_0).$$

Integrating between $\lambda = 0$ and $\lambda = L$, the bed volume of each segment

$$V = \int_0^L \frac{2}{3}\left[K_w K_d \lambda^2 + (K_w D_0 + K_d W_0)\lambda + W_0 D_0\right] d\lambda .$$

Solving and rearranging obtains

$$V = \frac{L}{3}\left(W_0 D_0 + \tfrac{1}{2}\Delta W D_0 + \tfrac{1}{2}\Delta D W_0 + \tfrac{1}{3}\Delta W \Delta D\right).$$

The same integration applies for channels with rectangular, triangular, or parabolic cross sections. However, volumes calculated using alternative cross-sections differ by the ratio of the areas of the approximating polygons, as presented in Table B.1.

TABLE B.1. Volume Scaling Factors for Cross-Sectional Profiles

Cross-section	Area	Factor
Rectangular	WD	1.00
Elliptical	¼ π WD	0.79
Parabolic	⅔ WD	0.67
Triangular	½ WD	0.50

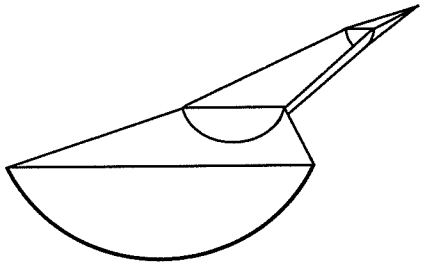

Figure B.1: Channel Sediment Volume Estimation. Widths are measured in the field, depths measured where possible, otherwise interpolated between bedrock exposures. Bottom cross-sections are assumed to be parabolic.

Channel Margin Sediment Volume Estimation.

The set of polyhedrons used to approximate channel-margin sediment volumes in the field is shown in Figure B.2. The corresponding volume formulae are listed in Table B.2.

TABLE B.2. Volume Formulae for Sediment Polyhedrons

Approximating polyhedron	Volume Formula
Half-cone (small debris fan)	$(0.38)^a \pi R^2 H/3$
Rectangular prism	LWH
Rectangular wedge	LWH/2
Triangular prism	LWH/2
Triangular wedge, tall point	LWH/6
Triangular wedge, tall base	LWH/3

[a] Experimentally determined coefficient

R radius
L length along channel
W width perpendicular to channel
H vertical thickness of deposit

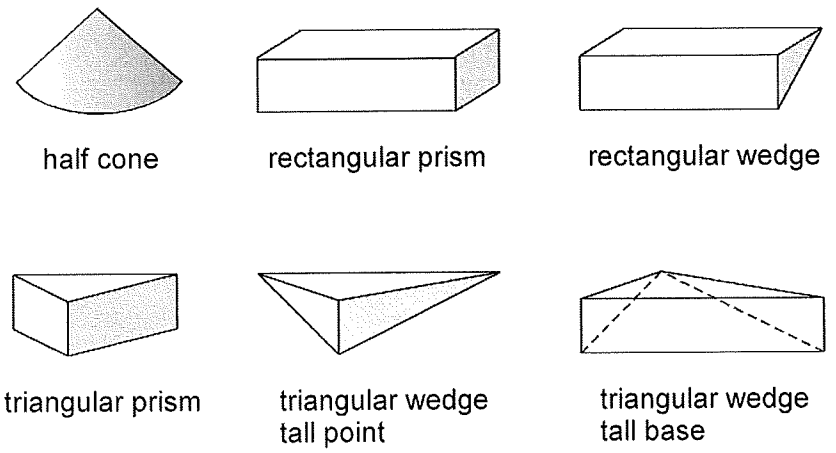

Figure B.2: Channel Margin Sediment Volume Approximation Polyhedrons.

Appendix C: Channel Profile Data

Bed Material: **G** gravel, **C** cobble, **B** boulder, **W** wood, **BR** bedrock
Bed Depth: **e** estimated/interpolated, otherwise measured directly

HR 6
Industrial Forest

upstream east-west coordinate (m) X	upstream north-south coordinate (m) Y	upstream length coordinate (m) L	upstream surface elevation (m) Z	section bed material M	upstream bed width (m) W	upstream bed depth (m) D	section bed volume (m^3) V_B	section sideslope volume (m^3) V_S
0.0	0.0	0.0	0.0	BR		0.0	0.0	0.0
8.4	23.0	24.5	-5.5	BR		0.0	0.0	0.0
10.2	28.1	29.9	-5.9	BR		0.0	0.0	0.0
12.1	33.1	35.2	-9.7	BR		0.0	0.0	0.0
15.1	41.4	44.0	-12.4	GCW	6.5	0.0 e	2.4	0.0
17.7	48.6	51.8	-13.6	BR	3.7	0.2	0.0	0.0
21.3	58.4	62.2	-14.7	BR		0.0	0.0	0.0
24.6	67.6	71.9	-16.9	BR		0.0	0.0	0.0
28.0	76.9	81.9	-18.1	BR		0.0	0.0	0.0
28.0	87.9	92.8	-19.3	BR		0.0	0.0	0.0
28.0	97.7	102.6	-21.3	BR		0.0	0.0	0.0
28.0	107.7	112.7	-25.8	BR		0.0	0.0	0.0
28.0	115.6	120.5	-27.3	BR		0.0	0.0	0.0
28.0	125.4	130.4	-31.9	BR		0.0	0.0	0.0
28.0	130.0	135.0	-35.1	BR		0.0	0.0	0.0
28.0	138.4	143.3	-36.8	BR		0.0	0.0	0.0
28.0	138.6	143.5	-37.0	BR		0.0	0.0	0.0
28.7	142.6	147.6	-39.0	BR		0.0	0.0	0.0
30.5	152.8	158.0	-40.2	BR		0.0	0.0	0.0
32.2	162.7	168.0	-40.9	BR		0.0	0.0	0.0
32.9	166.3	171.6	-44.3	BR		0.0	0.0	0.0
33.7	171.1	176.5	-45.3	BR		0.0	0.0	0.0
36.3	180.6	186.4	-47.0	BR		0.0	0.0	0.0
38.6	189.1	195.2	-48.9	GC	1.0	0.0 e	0.5	0.0
40.1	194.9	201.2	-49.2	C	6.1	0.1 e	0.8	0.0
43.6	200.9	208.2	-49.7	BR	4.0	0.0	0.0	0.0
45.7	204.6	212.4	-52.9	BR	3.0	0.0	0.0	0.0
49.6	211.3	220.1	-53.1	BR	4.3	0.0	0.0	0.0
54.6	219.9	230.1	-54.2	GCBW	4.0	0.0 e	4.0	0.0
57.5	224.9	235.9	-54.2	BR	4.9	0.5	0.0	0.0
60.6	234.6	246.0	-55.9	GC	3.3	0.0 e	3.7	0.0
61.8	238.3	249.9	-55.9	GCW	5.6	0.6 e	31.8	0.0
64.0	245.2	257.2	-56.3	GCW	8.7	1.2 e	9.4	0.0
64.8	247.5	259.5	-57.7	GCW	8.7	0.2 e	80.3	0.0
67.9	257.0	269.5	-57.5	LJ	14.3	1.8 e	175.4	0.0
70.9	266.4	279.5	-58.5	LJ	12.9	2.1 e	80.8	0.0
73.8	275.4	288.9	-61.8	LJ	9.0	0.1 e	2.7	0.0
76.9	284.8	298.8	-63.3	BR	4.5	0.0	0.0	0.0
82.6	293.0	308.8	-63.6	BR		0.0	0.0	0.0
89.4	302.7	320.6	-70.3	BR		0.0	0.0	0.0
93.4	308.3	327.5	-73.5	BR		0.0	0.0	0.0
100.4	318.4	339.8	-73.8	BR		0.0	0.0	0.0
103.8	323.2	345.7	-76.6	BR		0.0	0.0	0.0
108.1	329.4	353.3	-77.0	BR		0.0	0.0	0.0
114.9	339.0	365.0	-79.0	BR		0.0	0.0	0.0
122.1	349.4	377.7	-81.9	BR		0.0	0.0	0.0
126.4	355.4	385.0	-83.4	BR		0.0	0.0	0.0
127.1	358.1	387.8	-84.7	BR		0.0	0.0	0.0
130.7	371.7	401.8	-86.3	BR		0.0	0.0	0.0

upstream east-west coordinate (m) X	upstream north-south coordinate (m) Y	upstream length coordinate (m) L	upstream surface elevation (m) Z	section bed material M	upstream bed width (m) W	upstream bed depth (m) D	section bed volume (m^3) V_B	section sideslope volume (m^3) V_S
133.2	380.9	411.3	-89.5	BR		0.0	0.0	0.0
135.9	391.1	422.0	-90.5	GC	8.2	0.0 e	2.4	0.0
136.8	394.3	425.3	-90.5	GCW	6.5	0.3 e	1.8	0.0
137.5	397.0	428.0	-91.0	BR	5.9	0.0	0.0	0.0
141.1	410.5	442.1	-92.3	BR		0.0	0.0	0.0
142.8	416.8	448.6	-94.6	BR		0.0	0.0	0.0
145.4	426.5	458.6	-94.8	BR		0.0	0.0	8.0
145.6	427.3	459.5	-95.4	BR		0.0	0.0	0.0
145.6	436.8	468.9	-96.1	BR		0.0	0.0	0.0
145.6	441.6	473.8	-97.4	GCB	6.2	0.0 e	0.0	0.0
145.6	456.6	488.8	-98.0	BR	7.6	0.0	0.0	0.0
145.6	466.5	498.7	-99.3	BR	6.4	0.0	0.0	0.0
145.6	479.1	511.2	-108.8	GCW		0.0 e	0.0	0.0
145.6	489.1	521.2	-109.1	BR		0.0	0.0	0.0
145.6	498.9	531.1	-110.9	BR		0.0	0.0	0.0
150.6	507.6	541.1	-110.9	BR		0.0	0.0	0.0
155.6	516.2	551.0	-111.9	BR		0.0	0.0	0.0
160.4	524.6	560.7	-114.3	BR		0.0	0.0	0.0
164.1	531.0	568.1	-118.0	BR	5.7	0.0	0.0	13.7
167.5	536.9	574.9	-118.3	BR	9.0	0.0	0.0	0.0
172.9	546.1	585.6	-119.7	GCB	6.0	0.0 e	1.7	0.0
175.0	549.8	589.8	-119.9	GCB	7.3	0.2 e	17.0	0.0
180.0	558.4	599.7	-120.5	GCB	9.7	0.4 e	24.2	0.0
184.9	567.0	609.7	-121.4	BR	10.8	0.3	0.0	0.0
189.9	575.6	619.6	-122.6	BR		0.0	0.0	0.0
194.8	584.2	629.5	-124.3	BR		0.0	0.0	0.0
199.6	589.9	636.9	-125.9	BR		0.0	0.0	0.0
202.1	592.8	640.7	-129.2	BR		0.0	0.0	0.0
212.7	605.5	657.3	-130.9	BR		0.0	0.0	0.0
218.3	612.2	666.1	-132.0	BR		0.0	0.0	0.0
225.3	620.5	676.9	-134.9	BR		0.0	0.0	0.0
231.2	627.5	686.0	-136.0	BR		0.0	0.0	0.0
230.8	631.5	690.1	-138.4	BR		0.0	0.0	0.0
230.3	637.7	696.3	-141.2	BR		0.0	0.0	0.0
229.5	647.0	705.6	-141.5	BR		0.0	0.0	0.0
228.6	656.8	715.4	-143.3	BR		0.0	0.0	0.0
		725.2	-145.5		5.1		0.0	

HR 4

Industrial Forest

upstream east-west coordinate (m) X	upstream north-south coordinate (m) Y	upstream length coordinate (m) L	upstream surface elevation (m) Z	section bed material M	upstream bed width (m) W	upstream bed depth (m) D	section bed volume (m^3) V_B	section sideslope volume (m^3) V_S
0.0	0.0	0.0	0.0	CBW	3.0	2.0 e	17.9	0.0
2.7	8.4	8.9	-4.6	CBW	3.0	0.1 e	3.4	0.0
5.7	17.6	18.5	-7.4	CBW	5.0	0.2 e	15.5	0.0
8.7	26.8	28.2	-9.8	GCBW	5.0	0.8 e	14.5	0.0
11.5	35.5	37.3	-13.9	GCBW	3.0	0.4 e	10.3	4.0
14.5	44.7	47.0	-16.5	CB	5.0	0.4 e	12.2	0.0
16.9	51.9	54.6	-19.0	CBW	7.0	0.4 e	40.8	0.0
20.2	62.2	65.4	-20.9	CB	8.0	1.1 e	40.4	0.0
23.4	72.0	75.7	-24.8	CB	9.0	0.3 e	14.6	0.0
26.3	81.1	85.2	-27.7	BR	6.0	0.3	0.0	0.0

upstream east-west coordinate (m) X	upstream north-south coordinate (m) Y	upstream length coordinate (m) L	upstream surface elevation (m) Z	section bed material M	upstream bed width (m) W	upstream bed depth (m) D	section bed volume (m^3) V_B	section sideslope volume (m^3) V_S
29.3	90.3	94.9	-30.2	BR		0.0	0.0	0.0
25.8	97.9	103.4	-35.6	BR		0.0	0.0	0.0
22.4	105.3	111.5	-38.1	BR		0.0	0.0	0.0
17.0	116.8	124.1	-45.2	CBW	3.0	0.0 e	2.7	0.0
14.1	123.0	131.0	-46.6	GCB	6.0	0.2 e	8.8	0.0
10.0	131.8	140.7	-49.0	CBW	4.0	0.3 e	9.1	0.0
6.0	140.4	150.2	-52.1	CB	4.0	0.4 e	12.8	0.0
1.9	149.1	159.8	-54.8	CB	6.0	0.4 e	13.1	0.0
1.9	158.9	169.6	-56.8	CB	4.0	0.4 e	13.2	0.0
1.9	168.8	179.5	-58.4	BR	4.0	0.6	0.0	0.0
1.9	178.4	189.1	-61.1	BR	4.0	0.0	0.0	0.0
7.3	186.7	199.0	-63.0	BR		0.0	0.0	0.0
11.1	192.5	206.0	-65.6	BR		0.0	0.0	0.0
12.0	193.9	207.6	-69.3	BR		0.0	0.0	0.0
16.5	200.9	216.0	-70.9	BR		0.0	0.0	0.0
21.8	209.1	225.7	-73.0	CB		0.0 e	5.2	0.0
27.1	217.2	235.4	-75.5	CB		0.4 e	1.7	0.0
32.4	225.4	245.1	-77.8	BR	4.0	0.0	0.0	0.0
33.6	233.5	253.4	-81.5	BR		0.0	0.0	0.0
34.5	240.4	260.3	-82.6	BR		0.0	0.0	0.0
35.5	247.2	267.1	-83.9	BR		0.0	0.0	0.0
37.5	261.3	281.4	-92.3	GCB	3.0	0.0 e	0.0	0.0
38.4	267.7	287.8	-92.8	BR	5.0	0.0	0.0	0.0
39.7	277.4	297.7	-94.5	BR		0.0	0.0	0.0
41.2	287.9	308.3	-97.4	BR		0.0	0.0	0.0
42.4	296.5	316.9	-100.0	GCB	4.0	0.0 e	3.0	0.0
43.7	306.0	326.6	-102.7	BR	5.0	0.2	0.0	0.0
44.6	315.7	336.3	-104.8	BR		0.0	0.0	0.0
45.4	325.1	345.8	-108.1	BR	6.0	0.0	0.0	0.0
46.0	331.8	352.4	-110.3	BR	6.0	0.0	0.0	0.0
47.1	344.4	365.2	-113.0	BR	6.0	0.0	0.0	0.0
48.2	357.1	377.9	-115.6	BR	6.0	0.0	0.0	0.0
49.0	366.3	387.1	-119.5	BR	6.0	0.0	0.0	0.0
44.3	383.8	405.2	-123.5	BR	6.0	0.0	0.0	0.0
42.2	391.6	413.3	-126.0	BR	6.0	0.0	0.0	54.0
39.8	400.9	422.9	-128.8	BR	6.0	0.0	0.0	0.0
47.3	443.7	466.4	-135.3	?		0.0 e	1.7	0.0
48.9	453.0	475.8	-136.6	CB	2.0	0.4 e	2.9	0.0
50.6	462.3	485.2	-137.9	CB	3.0	0.0 e	2.9	0.0
51.9	469.5	492.5	-139.5	CB	3.0	0.4 e	8.3	0.0
53.7	479.7	502.9	-140.9	CB	3.0	0.4 e	3.8	0.0
60.7	486.1	512.4	-141.7	BR	3.0	0.0	0.0	0.0
68.0	492.6	522.2	-143.7	BR		0.0	0.0	0.0
69.4	500.8	530.5	-147.2	BR		0.0	0.0	0.0
71.1	510.3	540.2	-149.6	BR		0.0	0.0	0.0
73.0	520.8	550.9	-152.3	BR		0.0	0.0	0.0
76.5	541.1	571.5	-156.4	BR		0.0	0.0	0.0
78.2	550.5	580.9	-159.6	BR		0.0	0.0	0.0
80.6	564.1	594.8	-161.5	BR		0.0	0.0	14.9
82.1	572.7	603.5	-163.9	BR		0.0	0.0	0.0
83.7	582.0	613.0	-167.0	BR	7.0	0.0	0.0	0.0
87.2	601.4	632.7	-170.6	BR	3.0	0.0	0.0	0.0
89.7	610.9	642.5	-172.5	BR		0.0	0.0	0.0
92.2	620.4	652.3	-174.5	BR		0.0	0.0	0.0
94.8	629.8	662.1	-176.6	BR		0.0	0.0	0.0
96.8	637.3	669.8	-178.5	BR		0.0	0.0	0.0

upstream east-west coordinate (m) X	upstream north-south coordinate (m) Y	upstream length coordinate (m) L	upstream surface elevation (m) Z	section bed material M	upstream bed width (m) W	upstream bed depth (m) D	section bed volume (m^3) V_B	section sideslope volume (m^3) V_S
99.6	647.7	680.6	-180.6	BR	5.0	0.0	0.0	0.0
102.3	658.0	691.3	-183.5	BR	3.3	0.0	0.0	0.0
104.9	667.5	701.1	-185.2	BR		0.0	0.0	0.0
106.9	675.1	709.0	-186.4	BR		0.0	0.0	32.9
		720.9	-188.4					

HR 3

Industrial Forest

upstream east-west coordinate (m) X	upstream north-south coordinate (m) Y	upstream length coordinate (m) L	upstream surface elevation (m) Z	section bed material M	upstream bed width (m) W	upstream bed depth (m) D	section bed volume (m^3) V_B	section sideslope volume (m^3) V_S
0.0	0.0	0.0	0.0	BR		0.0	0.0	0.0
-1.9	7.1	7.3	-0.1	BR		0.0	0.0	0.0
-4.5	16.7	17.3	-1.0	BR		0.0	0.0	0.0
-5.8	21.5	22.2	-1.5	BR		0.0	0.0	0.0
-6.6	24.6	25.5	-5.3	BR		0.0	0.0	0.0
-11.6	33.0	35.3	-7.2	BR		0.0	0.0	0.0
-16.7	41.5	45.2	-8.9	BR		0.0	0.0	0.0
-21.8	50.0	55.1	-10.2	GCBW	0.0	0.0	0.0	0.0
-26.7	58.1	64.5	-13.4	BR	3.0	0.0	0.0	0.0
-31.8	66.5	74.4	-15.1	BR		0.0	0.0	0.0
-38.8	73.6	84.3	-16.3	BR		0.0	0.0	0.0
-45.9	80.6	94.3	-16.6	BR		0.0	0.0	0.0
-49.3	91.8	106.0	-19.3	BR		0.0	0.0	0.0
-49.4	92.3	106.5	-24.9	GCB	0.0	0.0 e	1.1	0.0
-51.9	100.4	115.0	-25.3	GCB	6.9	0.1 e	1.5	0.0
-58.5	105.0	123.0	-25.7	BR	5.5	0.0	0.0	0.0
-59.5	105.7	124.2	-30.1	BR		0.0	0.0	0.0
-64.4	109.1	130.2	-30.4	BR		0.0	0.0	0.0
-69.1	119.2	141.3	-35.0	BR		0.0	0.0	0.0
-75.3	132.7	156.2	-36.7	BR		0.0	0.0	0.0
-81.7	146.2	171.1	-37.8	BR		0.0	0.0	0.0
-78.2	158.1	183.5	-41.7	BR		0.0	0.0	0.0
-74.3	172.0	198.0	-45.7	BR		0.0	0.0	0.0
-70.2	186.2	212.7	-48.4	BR		0.0	0.0	0.0
-66.1	200.6	227.7	-49.5	BR		0.0	0.0	0.0
-58.7	210.8	240.3	-52.8	BR		0.0	0.0	0.0
-55.1	215.7	246.4	-55.1	BR		0.0	0.0	0.0
-49.0	224.1	256.7	-56.8	BR		0.0	0.0	0.0
-40.5	235.8	271.2	-60.8	GCB	0.0	0.0 e	38.2	0.0
-36.6	250.2	286.2	-61.6	GCB	8.0	1.4 e	146.3	0.0
-32.8	264.6	301.0	-63.6	GCB	11.4	1.6 e	189.7	81.1
-28.9	279.0	315.9	-65.5	GCB W	11.0	1.8 e	119.8	177.0
-24.6	295.3	332.8	-67.6	GCB W		2.2 e	171.3	0.0
-21.2	307.7	345.7	-69.0	LJ	16.0	2.6 e	237.6	0.0
-17.4	322.0	360.5	-71.5	GCBW	3.0	2.4 e	91.2	13.3
-8.1	338.1	379.1	-75.4	GCBW	5.6	1.2 e	5.1	0.0
-7.3	339.6	380.8	-76.4	GCBW	6.0	0.4 e	18.3	340.0
-0.8	350.8	393.7	-78.3	GCBW	5.0	0.4 e	16.7	0.0
0.5	365.6	408.5	-80.3	GCBW	5.9	0.2 e	9.3	0.0
1.8	380.4	423.4	-82.4	GCB	8.6	0.0 e	13.7	0.0
3.1	395.2	438.3	-84.0	GCB	8.4	0.3 e	27.6	0.0
9.4	407.6	452.1	-86.1	GCB	9.2	0.4 e	11.3	0.0

upstream east-west coordinate (m) X	upstream north-south coordinate (m) Y	upstream length coordinate (m) L	upstream surface elevation (m) Z	section bed material M	upstream bed width (m) W	upstream bed depth (m) D	section bed volume (m^3) V_B	section sideslope volume (m^3) V_S
13.4	415.5	461.1	-87.2	BR	10.0	0.0	0.0	0.0
13.8	416.3	462.0	-87.6	BR	10.0	0.0	0.0	0.0
16.0	420.6	466.8	-89.0	BR		0.0	0.0	0.0
16.7	424.5	470.7	-89.7	BR		0.0	0.0	0.0
19.6	441.0	487.5	-92.4	BR		0.0	0.0	0.0
22.5	457.5	504.3	-95.1	GCBW	0.0	0.0 e	47.8	0.0
25.1	472.3	519.2	-96.2	GCB	8.7	1.7 e	227.0	0.0
27.7	486.9	534.1	-98.0	GCB	12.3	2.6 e	262.4	0.0
36.9	490.7	544.1	-99.1	GCB	14.2	3.3 e	374.2	0.0
46.1	494.4	554.0	-100.3	GCB	16.6	4.0 e	530.9	0.0
55.3	498.1	563.9	-101.6	GCB	21.0	4.5 e	528.1	0.0
64.4	501.8	573.7	-103.6	GCB	15.5	4.3 e	625.8	0.0
76.4	506.6	586.6	-105.1	GCB	15.2	5.2 e	1269.1	0.0
89.7	519.9	605.5	-107.5	GCB	20.0	6.3 e	1011.0	0.0
98.7	529.0	618.3	-109.9	GCB	18.0	6.2 e	1484.0	0.0
95.3	548.4	638.0	-113.2	GCB	17.5	6.5 e	1517.9	0.0
91.9	567.9	657.8	-115.9	GCB	15.5	7.4 e	1081.6	0.0
88.4	587.4	677.5	-119.0	GCB	5.9	8.0 e	99.0	0.0
87.9	590.3	680.5	-119.3	GCB	6.3	8.3 e	1655.5	0.0
95.7	608.6	700.4	-121.5	GCB	21.0	9.7 e	1690.0	0.0
102.2	623.9	717.0	-125.0	GCBW	11.0	9.3 e	406.9	0.0
104.5	629.4	723.0	-125.9	LJ	11.0	9.5 e	1170.8	0.0
111.1	644.8	739.8	-128.5	GCB	10.5	10.0 e	1126.5	99.0
122.2	654.8	754.7	-129.7	GCBW	10.5	11.5 e	1559.2	0.0
134.6	666.1	771.5	-132.6	GCBW	13.5	11.7 e	1787.5	0.0
141.4	684.6	791.3	-135.5	GCBW	9.0	12.4 e	1605.5	0.0
148.1	703.2	811.0	-138.9	GCBW	10.5	12.6 e	337.5	0.0
149.5	706.9	814.9	-139.4	GCBW	9.5	12.9 e	1817.7	0.0
146.7	722.5	830.8	-141.3	GCBW	16.0	13.9 e	2724.7	0.0
143.4	741.1	849.7	-143.3	GCBW	13.5	15.4 e	2021.1	0.0
151.4	754.9	865.6	-145.2	GCBW	10.5	16.4 e	1207.8	0.0
158.8	767.8	880.5	-147.1	GCB	4.0	17.3 e	1473.8	143.1
157.1	787.6	900.4	-149.1	GCBW	8.2	18.9 e	2762.6	40.5
155.4	807.5	920.3	-150.6	GCBW	12.5	21.1 e	963.1	0.0
		932.3	-151.9		9.5			

HR 2

Industrial Forest

upstream east-west coordinate (m) X	upstream north-south coordinate (m) Y	upstream length coordinate (m) L	upstream surface elevation (m) Z	section bed material M	upstream bed width (m) W	upstream bed depth (m) D	section bed volume (m^3) V_B	section sideslope volume (m^3) V_S
0.0	0.0	0.0	0.0	GCBW	2.0	0.4 e	3.8	0.0
-8.9	-3.2	9.5	-3.2	GCBW	1.0	0.4 e	2.4	0.0
-15.8	-5.7	16.8	-5.2	GCBW	1.5	0.4 e	4.0	0.0
-27.1	-9.9	28.8	-8.3	GCBW	1.0	0.4 e	3.3	0.0
-36.3	-13.2	38.6	-10.2	GCW	1.5	0.4 e	2.4	0.0
-45.4	-16.5	48.3	-12.7	BR	2.5	0.0	0.0	0.0
-53.9	-19.6	57.3	-16.1	GCW	2.0	0.0 e	0.0	0.0
-59.8	-21.8	63.7	-16.9	BR	3.0	0.0	0.0	0.0
-62.6	-22.8	66.6	-19.6	CBW	3.0	0.0 e	3.8	0.0
-71.7	-26.1	76.3	-22.1	CBW	4.0	0.3 e	8.9	0.0
-80.8	-29.4	86.0	-24.6	GCBW	2.0	0.6 e	6.0	0.0
-89.6	-32.6	95.4	-28.1	BR	5.0	0.0	0.0	0.0

upstream east-west coordinate (m) X	upstream north-south coordinate (m) Y	upstream length coordinate (m) L	upstream surface elevation (m) Z	section bed material M	upstream bed width (m) W	upstream bed depth (m) D	section bed volume (m^3) V_B	section sideslope volume (m^3) V_S
-95.5	-26.7	103.7	-30.4	BR	3.8	0.0	0.0	0.0
-105.0	-17.3	117.1	-34.1	GCBW	3.0	0.0 e	0.0	0.0
-108.6	-13.6	122.2	-34.8	BR	0.0	0.0	0.0	0.0
-114.6	-7.6	130.7	-36.5	GCB	1.5	0.0 e	7.8	0.0
-116.9	0.9	139.6	-36.8	GCB	3.7	0.9 e	9.3	0.0
-119.2	9.3	148.3	-38.8	BR	3.5	0.0	0.0	0.0
-122.1	20.4	159.7	-40.0	BR	3.0	0.0	0.0	0.0
-122.8	22.9	162.3	-42.4	BR		0.0	0.0	0.0
-126.0	34.7	174.6	-44.5	BR		0.0	0.0	0.0
-127.6	40.6	180.7	-45.6	GCB	0.0	0.0 e	0.4	0.0
-128.2	43.2	183.3	-45.8	GCB	3.0	0.2 e	5.0	0.0
-129.6	48.3	188.6	-46.2	GCB	3.5	0.6 e	3.1	2.0
-130.8	52.8	193.3	-47.6	GCB	2.3	0.0 e	1.0	0.0
-137.8	59.3	202.9	-49.1	CB	3.5	0.1 e	0.1	0.0
-138.5	60.0	203.8	-49.4	BR	2.5	0.0	0.0	0.0
-142.7	63.9	209.5	-50.5	BR		0.0	0.0	0.0
-147.6	68.5	216.2	-51.4	BR		0.0	0.0	0.0
-150.3	71.0	219.9	-52.6	BR		0.0	0.0	0.0
-156.1	70.5	225.8	-57.9	BR		0.0	0.0	0.0
-165.7	69.6	235.4	-59.3	GCBW	2.0	0.0 e	1.2	0.0
-171.9	69.1	241.6	-59.9	CB		0.9 e	2.5	0.0
-176.3	68.7	246.1	-62.7	CB	3.0	0.4 e	4.1	0.0
-181.4	68.2	251.1	-64.2	CB	3.0	0.4 e	5.0	0.0
-194.5	67.1	264.3	-66.0	BR	2.5	0.0	0.0	0.0
-202.8	70.1	273.2	-67.4	BR		0.0	0.0	0.0
-212.1	73.5	283.0	-69.3	BR		0.0	0.0	0.0
-218.6	75.9	289.9	-70.2	GCB	6.0	0.0 e	5.4	0.0
-221.4	76.9	292.9	-69.9	GCB	7.0	0.8 e	32.0	0.0
-226.1	78.6	297.9	-70.2	GCB	10.0	1.4 e	26.2	0.0
-233.2	81.2	305.5	-72.7	GCB		0.3 e	0.4	0.0
-235.0	81.9	307.4	-73.4	BR	6.0	0.0	0.0	0.0
-244.6	80.8	317.0	-76.0	BR		0.0	0.0	0.0
-254.3	79.8	326.8	-78.0	BR		0.0	0.0	0.0
-264.0	78.8	336.5	-80.6	BR		0.0	0.0	0.0
-273.6	77.8	346.3	-82.8	BR		0.0	0.0	0.0
-276.4	77.5	349.1	-83.9	BR		0.0	0.0	0.0
-279.2	77.2	351.9	-84.9	BR		0.0	0.0	0.0
-284.9	74.8	358.1	-88.1	BR		0.0	0.0	0.0
-296.7	69.8	370.8	-90.7	BR		0.0	0.0	0.0
-299.3	68.7	373.7	-91.5	GCB	4.0	0.0 e	4.8	0.0
-305.7	66.0	380.7	-92.3	GCB	5.0	0.4 e	33.9	0.0
-314.9	62.1	390.6	-93.7	BR	11.0	0.8	0.0	0.0
-332.0	54.8	409.2	-97.3	BR		0.0	0.0	0.0
-340.3	50.8	418.4	-101.3	BR		0.0	0.0	0.0
-350.2	45.9	429.5	-105.9	BR		0.0	0.0	0.0
-357.4	42.4	437.4	-106.6	BR		0.0	0.0	0.0
-369.1	36.2	450.7	-109.1	BR		0.0	0.0	0.0
-373.8	33.7	456.0	-110.6	GCBW	0.0	0.0 e	3.4	0.0
-379.9	30.5	462.9	-111.7	GCBW	5.0	0.4 e	1.3	0.0
-381.5	29.6	464.7	-112.5	BR	5.0	0.0	0.0	0.0
-383.9	28.4	467.4	-113.8	GCBW	0.0	0.0 e	0.6	0.0
-386.5	26.9	470.4	-113.8	GCBW	2.5	0.4 e	1.3	0.0
-391.7	24.2	476.3	-114.8	BR	0.0	0.0	0.0	0.0
-401.0	24.2	485.6	-118.6	GCBW		0.0 e	10.4	0.0
-410.9	24.2	495.5	-120.0	GCBW	7.0	0.7 e	11.7	0.0
-415.7	24.2	500.3	-121.2	GCB	6.0	0.4 e	5.6	0.0

upstream east-west coordinate (m) X	upstream north-south coordinate (m) Y	upstream length coordinate (m) L	upstream surface elevation (m) Z	section bed material M	upstream bed width (m) W	upstream bed depth (m) D	section bed volume (m^3) V_B	section sideslope volume (m^3) V_S
-425.4	24.2	510.0	-123.6	GCB		0.0 e	3.1	0.0
-437.4	24.2	522.0	-124.3	GCB	7.0	0.2 e	1.5	0.0
-443.4	24.2	528.0	-124.9	BR		0.0	0.0	0.0
-453.3	24.2	538.0	-129.5	BR		0.0	0.0	0.0
-457.3	24.2	541.9	-130.0	BR		0.0	0.0	0.0
-467.3	24.2	551.9	-134.6	BR		0.0	0.0	0.0
-477.0	25.9	561.8	-135.9	BR		0.0	0.0	0.0
-486.8	27.6	571.7	-137.6	BR		0.0	0.0	0.0
-508.4	31.4	593.7	-138.0	CB	2.0	0.0 e	4.7	0.0
-517.9	33.1	603.3	-140.8	GCB	4.5	0.4 e	29.2	0.0
-529.5	31.0	615.1	-142.9	GCBW	7.0	0.9 e	11.2	0.0
-537.7	32.8	623.5	-146.1	BR		0.0	0.0	0.0
-548.2	35.0	634.1	-148.9	BR		0.0	0.0	0.0
-553.4	36.1	639.5	-150.2	GCBW	4.5	0.0 e	1.9	0.0
-559.7	37.5	646.0	-150.5	GCB		0.6 e	4.3	0.0
-563.6	38.3	650.0	-150.8	LJ	4.5	0.8 e	0.6	0.0
-564.1	38.4	650.5	-151.7	BR	4.5	0.0	0.0	0.0
-567.1	39.0	653.5	-151.7	GCBW	5.0	0.0 e	9.4	0.0
-577.9	43.6	665.2	-154.0	BR	3.5	0.6	0.0	2.3
-588.6	48.2	676.8	-157.1	GCB		0.6 e	3.5	1.7
-592.2	49.7	680.8	-157.3	GCB	4.0	0.7 e	16.0	0.0
-600.5	53.2	689.8	-158.1	GCW	5.5	0.4 e	0.7	0.0
-601.3	53.6	690.7	-158.6	BR	5.0	0.0	0.0	0.0
-610.5	57.3	700.6	-160.0	BR		0.0	0.0	0.0
-613.9	58.7	704.3	-163.4	BR		0.0	0.0	0.0
-623.1	62.4	714.1	-165.0	BR		0.0	0.0	0.0
-628.9	64.7	720.4	-168.0	BR		0.0	0.0	0.0
-638.1	68.4	730.4	-169.0	BR		0.0	0.0	0.0
-642.6	68.0	734.8	-171.3	GCB		0.0 e	0.0	0.0
-645.5	67.7	737.8	-171.2	LJ		0.8 e	0.0	0.0
-646.1	67.6	738.4	-172.0	BR		0.0	0.0	0.0
-649.6	67.2	741.9	-173.9	GC		0.0 e	0.0	0.0
-658.4	66.3	750.8	-175.2	GC		0.2 e	0.0	0.0
-679.3	64.1	771.8	-175.5	LJ		3.3 e	33.2	0.0
-687.6	66.3	780.3	-178.3	GCBW	5.0	1.9 e	35.9	0.0
-693.2	67.8	786.2	-179.6	GCBW	6.0	1.5 e	18.1	0.0
-697.0	68.9	790.1	-180.5	LJ	4.0	1.3 e	5.1	0.0
-701.4	70.0	794.7	-182.5	BR		0.0	0.0	0.0
-704.3	70.8	797.6	-183.0	BR		0.0	0.0	0.0
-712.7	72.1	806.2	-185.8	GCB	0.0	0.0 e	3.2	0.0
-723.5	73.9	817.1	-187.1	GCB	5.0	0.3 e	6.2	0.0
-731.8	75.2	825.5	-188.5	GCB	8.0	0.1 e	14.9	0.0
-738.2	76.2	832.0	-188.8	GCB	9.5	0.7 e	99.6	61.9
-748.1	77.7	842.0	-188.8	GCB	12.0	2.0 e	243.6	28.8
-759.9	79.6	854.0	-189.7	GCB	13.0	2.8 e	208.8	0.0
-769.3	81.8	863.6	-192.2	GCB	15.9	1.7 e	174.0	0.0
-780.0	84.3	874.6	-193.3	GCB	9.0	2.2 e	132.0	0.0
-788.3	89.6	884.5	-194.8	GCB	10.0	2.0 e	129.2	0.0
-796.6	95.0	894.4	-196.3	GCB	9.8	1.9 e	129.8	0.0
-804.9	100.4	904.2	-197.9	GCB	12.0	1.7 e	147.6	0.0
-813.2	105.8	914.2	-199.2	GCB	13.0	1.9 e	121.3	0.0
-821.5	111.2	924.0	-200.7	GCB	7.5	1.7 e	114.0	0.0
-834.3	118.6	938.8	-203.2	GCB	7.5	1.4 e	87.9	0.0
-842.8	123.5	948.7	-204.8	GCB	14.0	1.1 e	112.5	0.0
-851.4	128.5	958.6	-206.0	GCB	14.0	1.3 e	223.3	0.0
-868.6	138.4	978.4	-209.0	GCB	14.0	1.1 e	250.3	0.0

upstream east-west coordinate (m) X	upstream north-south coordinate (m) Y	upstream length coordinate (m) L	upstream surface elevation (m) Z	section bed material M	upstream bed width (m) W	upstream bed depth (m) D	section bed volume (m^3) V_B	section sideslope volume (m^3) V_S
-883.2	146.8	995.3	-210.7	GCW	16.0	1.8 e	233.6	0.0
-893.1	163.9	1015.0	-214.0	GCB	6.3	1.3 e	111.5	141.0
-903.0	181.1	1034.9	-216.5	GCB	5.6	1.5 e	97.7	144.0
-912.8	198.2	1054.6	-219.8	GCB	6.0	1.0 e	54.1	171.0
-920.3	211.0	1069.5	-221.8	GCBW	4.2	1.1 e	1.4	75.0
-920.7	211.8	1070.3	-222.9	GCB	3.5	0.1 e	128.5	735.0
-932.7	232.5	1094.3	-224.4	GCBW	9.6	2.0 e	244.8	666.0
-939.5	251.2	1114.1	-226.9	GCB	7.5	2.3 e	164.9	187.5
-944.6	265.2	1129.1	-228.3	GCB	5.0	3.0 e	414.8	200.0
-951.3	283.7	1148.7	-231.9	GCB	20.0	2.2 e	355.0	0.0
-956.4	297.7	1163.6	-234.1	GCB	13.0	2.1 e	266.9	0.0
-961.5	311.7	1178.5	-235.8	GCB	10.0	2.5 e	146.0	0.0
		1193.4	-237.3	GCB	14.6			

HR 1

Old-growth Forest, transition to Industrial Forest at 646.9 m length

upstream east-west coordinate (m) X	upstream north-south coordinate (m) Y	upstream length coordinate (m) L	upstream surface elevation (m) Z	section bed material M	upstream bed width (m) W	upstream bed depth (m) D	section bed volume (m^3) V_B	section sideslope volume (m^3) V_S
0.0	0.0	0.0	0.0	GCB	3.8	0.0 e	3.7	0.0
-6.5	4.6	8.0	-4.4	GCBW	2.4	0.5 e	0.8	0.0
-9.2	6.4	11.2	-6.8	GCW	0.0	0.0 e	0.0	0.0
-16.9	11.8	20.6	-9.5	GCW	2.5	0.0 e	0.0	0.0
-18.9	13.2	23.0	-10.8	GCBW	3.5	0.0 e	3.4	0.0
-25.0	17.5	30.5	-12.1	GCBW	3.0	0.4 e	3.6	0.0
-32.9	23.1	40.2	-14.6	BR	1.7	0.0	0.0	0.0
-40.3	28.2	49.2	-19.0	GCBW	2.0	0.0 e	10.2	0.0
-41.0	32.3	53.3	-18.1	GCBW	5.9	1.6 e	18.2	0.0
-42.1	38.6	59.8	-20.8	BR	3.8	0.0	0.0	0.0
-43.5	46.2	67.4	-25.1	BR	4.0	0.0	0.0	0.0
-44.4	51.2	72.5	-27.4	CW	5.0	0.0 e	0.0	0.0
-45.0	55.0	76.3	-30.8	GCW	7.0	0.0 e	49.9	0.0
-46.6	63.9	85.4	-32.7	GCW	9.0	2.0 e	36.7	0.0
-47.6	69.5	91.1	-36.9	GCW	8.0	0.3 e	88.6	0.0
-54.6	76.4	101.0	-38.5	LJ	8.5	3.0 e	56.8	0.0
-59.7	81.6	108.3	-46.4	GCBW	4.3	0.4 e	6.2	0.0
-62.4	84.3	112.0	-48.4	GCBW	8.3	0.4 e	18.3	0.0
-69.2	91.1	121.6	-51.1	CBW	6.0	0.4 e	12.8	0.0
-73.7	95.6	128.0	-52.4	CBW	5.0	0.7 e	0.0	0.0
-73.7	95.6	128.0	-53.8	GCW	5.3	0.4 e	59.5	40.8
-82.1	103.9	139.8	-56.2	GCBW	7.0	2.0 e	29.3	0.0
-82.5	106.6	142.6	-56.8	LJ	7.1	2.6 e	25.2	0.0
-83.5	111.9	147.9	-61.7	BR	2.4	0.0	0.0	0.0
-84.4	117.1	153.2	-63.8	GCW	2.9	0.0 e	8.5	0.0
-85.4	122.8	159.0	-64.4	GCW	3.4	1.4 e	15.7	0.0
-86.7	130.3	166.6	-68.0	GCBW	4.0	0.3 e	28.6	0.0
-91.6	138.8	176.4	-70.3	GCBW	6.0	1.4 e	72.7	0.0
-96.5	147.2	186.2	-72.3	GCBW	5.1	2.7 e	113.3	0.0
-101.4	155.8	196.0	-74.0	CBW	4.7	4.4 e	97.7	0.0
-105.9	163.6	205.1	-78.2	GCW	3.7	3.3 e	77.1	0.0
-109.4	169.6	212.0	-79.3	GCW	4.9	4.5 e	78.1	0.0
-112.0	174.2	217.3	-84.5	GCW	12.9	1.0 e	51.1	0.0
-118.7	185.7	230.5	-90.1	LJ	7.2	0.0 e	0.0	0.0

upstream east-west coordinate (m) X	upstream north-south coordinate (m) Y	upstream length coordinate (m) L	upstream surface elevation (m) Z	section bed material M	upstream bed width (m) W	upstream bed depth (m) D	section bed volume (m^3) V_B	section sideslope volume (m^3) V_S
-117.3	201.5	246.5	-94.7	BR	3.5	0.0	0.0	0.0
-116.7	208.2	253.1	-96.4	GCBW	0.0	0.0 e	0.7	0.0
-116.5	211.0	256.0	-96.7	GCBW	3.0	0.4 e	15.6	0.0
-115.7	219.8	264.8	-97.9	GCBW	3.4	1.2 e	11.6	0.0
-115.0	227.4	272.4	-100.6	GCBW	2.5	0.2 e	9.5	0.0
-114.2	236.9	281.9	-102.4	GCBW	4.5	0.6 e	3.2	0.0
-113.8	241.1	286.2	-104.0	BR	2.8	0.0	0.0	0.0
-112.7	254.3	299.4	-107.1	GCBW	0.0	0.0 e	3.5	0.0
-112.0	261.5	306.7	-108.0	BR	4.4	0.5	0.0	0.0
-111.5	268.1	313.3	-111.0	BR	0.0	0.0	0.0	0.0
-110.4	280.4	325.6	-114.1	BR		0.0	0.0	0.0
-110.9	281.2	326.6	-114.1	BR		0.0	0.0	0.0
-118.5	292.9	340.6	-118.0	BR		0.0	0.0	0.0
-118.9	297.5	345.1	-118.7	BR		0.0	0.0	0.0
-120.0	309.3	357.1	-123.8	BR		0.0	0.0	0.0
-121.2	322.8	370.5	-127.1	BR	0.0	0.0	0.0	0.0
-120.4	333.1	380.8	-128.9	GCB	4.7	0.8 e	30.2	0.0
-119.2	350.4	398.3	-132.3	GCBW	5.6	0.8 e	136.1	0.0
-117.6	373.3	421.2	-136.6	GCBW	8.6	1.5 e	129.8	0.0
-116.6	388.0	435.9	-139.0	GCW	8.0	2.3 e	74.6	0.0
-116.1	394.1	442.0	-140.1	LJ	6.5	2.6 e	53.6	0.0
-115.6	399.8	447.8	-142.4	LJ	5.5	1.5 e	7.6	0.0
-115.4	402.0	450.0	-144.6	LJ	3.5	0.4 e	11.6	0.0
-114.2	415.5	463.5	-146.8	BR	0.0	0.6	0.0	0.0
-113.9	419.3	467.4	-149.0	BR	0.0	0.0	0.0	0.0
-112.6	433.7	481.8	-151.2	GC	7.0	0.0 e	20.8	0.0
-111.6	445.5	493.6	-152.7	GCW	9.7	0.8 e	90.0	0.0
-110.3	460.3	508.5	-154.8	LJ	8.0	1.6 e	36.5	0.0
-107.5	470.7	519.2	-158.5	BR	0.0	0.0	0.0	0.0
-104.8	480.6	529.5	-160.1	BR	0.0	0.0	0.0	8.9
-103.1	487.2	536.3	-161.6	BR		0.0	0.0	0.0
-100.2	497.8	547.3	-165.8	BR		0.0	0.0	0.0
-97.1	509.6	559.5	-168.8	GCB	7.7	0.0 e	9.5	0.0
-94.6	518.6	568.9	-170.9	GCB	7.6	0.4 e	22.5	0.0
-97.3	531.1	581.7	-172.5	GCB	5.5	0.4 e	30.7	0.0
-99.8	542.9	593.7	-173.8	GCB	9.5	0.5 e	19.8	72.0
-102.6	555.9	607.0	-177.0	GCB	4.5	0.4 e	44.6	0.0
-105.8	570.9	622.4	-178.5	GCB	9.8	0.5 e	71.1	0.0
-108.4	583.5	635.2	-180.1	LJ	9.1	1.8 e	46.2	0.0
-107.4	595.2	646.9	-184.5	BR	0.0	0.0	0.0	0.0
-106.2	608.5	660.3	-186.1	BR		0.0	0.0	0.0
-105.1	621.6	673.4	-188.9	BR		0.0	0.0	0.0
-103.9	634.9	686.7	-190.7	BR		0.0	0.0	7.0
-102.9	646.2	698.2	-193.0	BR	0.0	0.0	0.0	0.0
-102.2	654.1	706.1	-194.6	GCB	5.0	0.0 e	0.0	0.0
-101.5	663.0	715.0	-195.4	BR	0.0	0.0	0.0	0.0
-101.1	667.4	719.5	-196.1	BR		0.0	0.0	0.0
-102.7	674.0	726.2	-197.8	BR		0.0	0.0	0.0
-105.7	685.9	738.5	-200.3	BR		0.0	0.0	0.0
-103.4	690.4	743.5	-201.9	BR		0.0	0.0	0.0
-97.2	702.5	757.1	-204.4	BR	0.0	0.0	0.0	0.0
-87.3	722.0	779.1	-205.4	GC	9.0	0.5 e	20.4	0.0
-78.0	740.2	799.4	-210.5	BR	0.0	0.0	0.0	10.7
-71.6	752.9	813.7	-212.2	BR		0.0	0.0	0.0
-63.1	769.4	832.3	-216.6	BR		0.0	0.0	0.0
-58.4	776.2	840.5	-217.8	BR		0.0	0.0	0.0

upstream east-west coordinate (m) X	upstream north-south coordinate (m) Y	upstream length coordinate (m) L	upstream surface elevation (m) Z	section bed material M	upstream bed width (m) W	upstream bed depth (m) D	section bed volume (m^3) V_B	section sideslope volume (m^3) V_S
-51.7	785.8	852.2	-219.3	BR		0.0	0.0	0.0
-47.9	791.1	858.7	-220.6	BR	0.0	0.0	0.0	8.6
-41.7	800.0	869.5	-221.9	LJ	8.2	0.0 e	7.1	0.0
-38.9	804.0	874.4	-223.1	LJ	8.0	0.5 e	9.6	0.0
-33.9	812.7	884.5	-227.1	BR	0.0	0.0	0.0	25.0
-28.8	821.6	894.8	-228.0	BR		0.0	0.0	0.0
-23.9	830.1	904.5	-229.6	BR	0.0	0.0	0.0	23.8
-15.5	844.6	921.3	-231.9	GCB	11.0	0.0 e	18.5	0.0
-16.4	862.2	939.0	-234.2	GCB	11.3	0.3 e	122.1	0.0
-17.8	888.7	965.5	-237.4	GCB	13.8	0.8 e	320.3	0.0
-19.0	910.8	987.7	-239.1	GCB	13.8	2.3 e	478.8	0.0
-20.1	932.8	1009.6	-242.5	GCB	16.0	2.1 e	390.6	0.0
-19.5	949.6	1026.5	-244.5	GCB	15.0	2.4 e	382.9	0.0
-18.8	970.1	1047.0	-248.7	GCB	16.0	1.2 e	49.5	0.0
-18.8	978.3	1055.2	-251.1	BR	14.2	0.0	0.0	0.0
-18.8	992.8	1069.6	-258.2	GCBW	11.0	0.0 e	20.2	0.0
-18.8	1005.5	1082.3	-261.0	GCBW	12.3	0.4 e	34.1	0.0
-18.8	1017.5	1094.4	-263.0	GCBW	9.0	0.4 e	28.6	0.0
-18.8	1028.6	1105.5	-265.1	GCBW	7.0	0.4 e	8.4	0.0
-18.8	1036.4	1113.2	-266.1	BR	6.3	0.0	0.0	0.0
-18.8	1041.1	1118.0	-268.3	BR	6.0	0.0	0.0	0.0
-18.8	1048.9	1125.8	-269.3	GC	4.2	0.0 e	7.0	0.0
-18.8	1060.1	1137.0	-270.8	GCB	4.0	0.4 e	11.8	0.0
-18.8	1067.9	1144.7	-271.8	GCB	6.0	0.5 e	10.3	0.0
-18.8	1073.9	1150.8	-272.7	GCB	7.7	0.4 e	18.9	0.0
-18.8	1078.3	1155.1	-272.6	GCBW	11.5	1.0 e	36.4	0.0
-17.5	1085.9	1162.9	-274.1	GCBW	10.0	0.6 e	28.0	0.0
-16.1	1093.5	1170.6	-276.1	GCBW	10.7	0.4 e	20.8	0.0
-14.9	1100.5	1177.7	-276.9	GCBW	12.0	0.4 e	10.0	0.0
-13.8	1106.8	1184.1	-277.5	GCBW	10.8	0.0 e	15.0	0.0
-8.4	1116.2	1194.9	-281.0	GCB	7.8	0.4 e	29.2	0.0
-3.1	1125.3	1205.4	-280.9	GCB	10.0	0.4 e	17.9	0.0
3.2	1136.2	1218.1	-282.1	GCB	11.0	0.1 e	20.8	0.0
9.5	1147.2	1230.7	-283.4	GCBW	9.0	0.5 e	30.3	0.0
14.3	1155.3	1240.1	-285.4	GCBW	11.3	0.4 e	28.3	0.0
19.9	1165.1	1251.4	-286.9	GCB	7.8	0.4 e	25.2	0.0
26.7	1176.8	1264.9	-288.4	GCB	10.4	0.2 e	4.7	0.0
29.5	1181.7	1270.6	-289.3	GCB	9.4	0.1 e	12.4	0.0
32.4	1186.8	1276.4	-289.5	GCB	10.2	0.6 e	24.4	0.0
31.6	1192.7	1282.4	-290.3	GCBW	9.7	0.6 e	23.6	0.0
30.4	1201.1	1290.9	-291.2	GCBW	7.0	0.4 e	14.1	0.0
29.3	1208.7	1298.6	-292.3	BR	8.0	0.2 e	4.7	0.0
28.2	1216.3	1306.3	-292.8	GCB	8.0	0.0	0.0	0.0
27.4	1222.3	1312.3	-293.5	GCB	7.8	0.4 e	9.6	0.0
26.6	1228.2	1318.3	-293.8	GCBW	5.6	0.3 e	24.8	0.0
21.0	1236.8	1328.5	-295.7	GCB	12.6	0.4 e	41.7	0.0
11.0	1252.2	1346.9	-298.4	BR	9.2	0.4 e	14.9	0.0
6.1	1259.8	1355.9	-299.3	GCB	11.5	0.2	0.0	0.0
1.9	1266.2	1363.6	-300.6	BR	10.2	0.0 e	0.0	0.0
-6.0	1278.4	1378.1	-302.9	BR	12.0	0.0	0.0	0.0
-12.8	1288.8	1390.5	-304.9	BR	8.0	0.0	0.0	64.1
-20.0	1299.9	1403.8	-306.5	BR	10.8	0.0	0.0	0.0
-25.7	1308.0	1413.7	-308.5	BR	8.4	0.0	0.0	0.0
-30.4	1314.8	1421.9	-309.2	GCB	6.4	0.0	0.0	0.0
-33.2	1318.8	1426.9	-311.0	GCB	9.8	0.0 e	0.2	0.0
-38.5	1326.4	1436.1	-313.5	BR	12.4	0.0 e	16.2	0.0

upstream east-west coordinate (m) X	upstream north-south coordinate (m) Y	upstream length coordinate (m) L	upstream surface elevation (m) Z	section bed material M	upstream bed width (m) W	upstream bed depth (m) D	section bed volume (m^3) V_B	section sideslope volume (m^3) V_S
-43.5	1333.5	1444.7	-314.9	GCBW	5.2	1.0	0.0	0.0
-43.5	1344.9	1456.2	-315.7	BR	5.9	0.0 e	6.4	0.0
-43.5	1354.4	1465.7	-316.9	GCB	9.0	0.2	0.0	0.0
-43.5	1365.8	1477.1	-318.5	GCB	10.0	0.0 e	1.1	0.0
-43.5	1370.5	1481.8	-319.1	B	7.0	0.1 e	1.1	0.0
-43.6	1371.3	1482.6	-320.7	GCB	6.9	0.4 e	18.1	0.0
-44.8	1379.6	1491.0	-320.9	GCB	6.2	0.4 e	13.4	0.0
-46.2	1389.6	1501.1	-322.1	GCB	8.5	0.1 e	12.1	0.0
-47.2	1397.1	1508.6	-323.5	GCB	11.0	0.4 e	17.8	0.0
-51.1	1404.7	1517.2	-325.6	GCB	9.4	0.4 e	33.7	0.0
-57.5	1417.2	1531.2	-327.3	GCB	9.5	0.4 e	51.2	0.0
-65.4	1432.7	1548.6	-330.1	GCB	11.0	0.4 e	36.0	114.4
-70.9	1443.5	1560.7	-332.9	GCB	13.0	0.4 e	67.8	292.3
-76.9	1455.3	1573.9	-333.1	GCB	23.5	0.5 e	112.5	40.5
-82.1	1465.4	1585.4	-334.2	GCB	22.0	1.2 e	56.1	248.9
		1595.9	-335.5					

HR 5

Old-growth Forest

upstream east-west coordinate (m) X	upstream north-south coordinate (m) Y	upstream length coordinate (m) L	upstream surface elevation (m) Z	section bed material M	upstream bed width (m) W	upstream bed depth (m) D	section bed volume (m^3) V_B	section sideslope volume (m^3) V_S
0.0	0.0	0.0	0.0	GCBW	3.5	0.0 e	21.5	0.0
-1.2	13.5	13.6	-2.8	GCBW	6.7	0.8 e	35.8	0.0
-2.0	23.2	23.3	-4.8	GCBW	9.0	0.6 e	40.8	0.0
-2.9	33.0	33.2	-6.8	GCB	7.3	1.0 e	107.1	0.0
-4.2	47.8	48.0	-9.9	GCBW	8.4	1.8 e	83.5	0.0
-5.0	57.5	57.8	-11.9	GCBW	6.9	1.6 e	88.2	0.0
-5.9	67.3	67.6	-13.9	GCBW	9.0	1.8 e	71.1	0.0
-4.2	76.7	77.1	-15.8	GCBW	8.0	0.8 e	37.7	0.0
-2.5	86.4	87.0	-17.9	GCBW	5.3	0.9 e	27.7	0.0
-0.8	96.4	97.2	-19.9	BR	6.1	0.5	0.0	0.0
0.0	100.8	101.6	-23.7	BR	1.5	0.0	0.0	0.0
1.5	109.4	110.3	-24.7	BR	4.0	0.0	0.0	0.0
3.1	118.5	119.5	-27.2	BR	3.9	0.0	0.0	0.0
4.8	128.2	129.4	-28.9	BR	4.7	0.0	0.0	0.0
6.6	138.0	139.3	-30.2	BR	6.9	0.0	0.0	0.0
8.3	147.5	149.0	-32.5	BR	7.3	0.0	0.0	0.0
9.9	157.1	158.8	-35.2	GCBW	8.5	0.5 e	31.1	0.0
11.5	166.1	167.8	-36.4	GCBW	9.4	0.6 e	1.1	0.0
11.6	166.6	168.4	-36.4	BR	9.4	0.0	0.0	0.0
13.3	176.3	178.2	-38.3	CBW	8.8	0.0 e	0.0	0.0
15.0	185.7	187.8	-41.0	BR	6.0	0.0	0.0	0.0
16.7	195.5	197.7	-42.5	GCBW	11.0	0.0 e	6.0	0.0
18.4	205.1	207.5	-44.8	GCBW	10.2	0.2 e	11.5	0.0
20.1	214.7	217.2	-47.1	CBW	5.1	0.3 e	16.3	0.0
21.8	224.4	227.1	-48.9	CB	8.9	0.4 e	23.9	0.0
24.3	233.8	236.8	-51.4	GCBW	9.6	0.4 e	16.8	0.0
27.2	244.5	247.9	-53.2	GCBW	9.1	0.1 e	17.1	0.0
29.4	252.8	256.5	-54.9	GCBW	9.3	0.6 e	25.8	0.0
31.9	262.3	266.3	-56.9	GCBW	6.5	0.4 e	15.9	0.0
34.5	271.7	276.1	-58.9	GCB	5.1	0.4 e	34.0	0.0
37.0	281.3	286.0	-60.9	CB	7.9	1.1 e	9.9	0.0

upstream east-west coordinate (m) X	upstream north-south coordinate (m) Y	upstream length coordinate (m) L	upstream surface elevation (m) Z	section bed material M	upstream bed width (m) W	upstream bed depth (m) D	section bed volume (m^3) V_B	section sideslope volume (m^3) V_S
37.0	284.3	289.0	-61.6	CB	10.4	0.0 e	23.4	0.0
37.0	291.1	295.7	-63.5	BR	10.4	1.0	0.0	0.0
37.0	301.5	306.1	-66.0	GCBW	8.4	1.0 e	21.0	0.0
37.0	310.2	314.9	-67.0	BR	4.7	0.0	0.0	0.0
37.0	320.2	324.9	-68.2	BR	5.8	0.0	0.0	0.0
37.0	331.2	335.8	-68.6	BR	8.1	0.0	0.0	0.0
37.0	338.1	342.8	-69.8	BR	5.5	0.0	0.0	0.0
37.0	344.7	349.4	-75.9	GCBW	6.8	1.0 e	160.8	0.0
41.7	357.4	362.9	-79.1	GCBW	13.7	2.3 e	354.9	0.0
45.1	366.7	372.8	-81.4	GCBW	19.3	4.0 e	588.9	0.0
48.5	376.0	382.7	-83.7	GCBW	20.6	4.9 e	795.0	0.0
51.9	385.4	392.7	-86.1	GCBW	21.9	6.3 e	1045.7	0.0
55.3	394.7	402.6	-88.4	GCBW	23.2	7.6 e	1447.6	0.0
58.6	404.0	412.5	-90.7	LJ	31.7	8.4 e	1630.9	0.0
62.0	413.2	422.3	-93.0	LJ	28.4	8.4 e	1381.4	0.0
58.7	422.2	431.9	-95.2	LJ	24.4	7.9 e	1163.1	0.0
55.4	431.2	441.4	-97.5	LJ	24.4	7.1 e	1308.0	0.0
52.0	440.4	451.3	-99.8	LJ	29.4	7.7 e	1312.8	0.0
49.1	448.6	459.9	-101.8	LJ	31.1	7.3 e	1429.4	0.0
45.3	459.0	471.1	-104.4	LJ	21.2	7.4 e	852.6	0.0
42.4	466.9	479.4	-106.4	LJ	20.5	7.3 e	560.2	0.0
38.3	478.3	491.5	-109.9	GCBW	13.4	0.4 e	18.4	0.0
34.4	488.9	502.8	-111.9	BR	9.9	0.0	0.0	0.0
30.0	501.1	515.9	-115.3	BR	10.2	0.0	0.0	13.0
26.6	510.4	525.7	-117.2	BR	8.8	0.0	0.0	0.0
23.5	518.8	534.7	-119.8	GCBW	5.5	0.0 e	24.7	0.0
19.9	528.7	545.2	-121.9	GCBW	8.8	0.9 e	88.4	0.0
19.9	540.6	557.1	-124.4	GCBW	7.4	1.9 e	12.8	0.0
19.9	542.6	559.1	-124.8	GCBW	7.4	0.7 e	35.4	0.0
19.9	548.1	564.6	-125.9	CBW	7.2	1.9 e	58.3	0.0
19.9	560.7	577.2	-128.5	GCB	7.6	0.0 e	31.0	26.5
15.5	572.8	590.1	-130.7	B	9.1	0.8 e	7.9	0.0
14.3	576.0	593.5	-131.3	GCBW	6.6	0.0 e	27.3	0.0
10.6	586.1	604.3	-133.2	GCBW	8.1	1.0 e	0.2	0.0
10.6	586.2	604.3	-134.0	CBW	8.1	0.4 e	19.1	0.0
7.6	594.4	613.0	-135.3	CBW	8.3	0.4 e	5.7	0.0
6.9	597.0	615.7	-136.5	CBW	7.4	0.4 e	3.5	0.0
6.0	600.5	619.4	-137.5	CBW	7.0	0.0 e	2.5	0.0
5.2	603.5	622.5	-137.9	GCBW	6.8	0.3 e	20.3	0.0
2.6	613.1	632.4	-139.3	BR	7.6	0.5	0.0	0.0
0.2	622.2	641.9	-142.0	BR		0.0	0.0	0.0
-2.2	631.1	651.1	-145.9	BR		0.0	0.0	0.0
-4.8	640.8	661.1	-145.7	BR		0.0	0.0	0.0
-6.4	646.9	667.4	-147.9	GCB	5.5	0.0 e	16.7	0.0
-5.2	661.3	681.9	-150.2	BR	5.9	0.6	0.0	0.0
-4.5	668.8	689.4	-151.9	GCB	7.1	0.6 e	46.1	0.0
-3.6	679.7	700.4	-153.3	GCBW	9.4	0.9 e	62.2	0.0
-2.7	689.6	710.3	-154.5	GCBW	10.2	1.0 e	73.6	0.0
-1.8	699.5	720.2	-156.2	CB	11.1	1.1 e	71.5	0.0
-1.0	709.2	730.0	-158.0	GCBW	12.0	0.8 e	60.9	0.0
-0.1	719.0	739.8	-159.7	GCBW	11.2	0.8 e	53.6	0.0
0.7	728.8	749.6	-161.4	CBW	10.6	0.7 e	24.7	0.0
1.6	738.5	759.4	-163.1	GCBW	11.5	0.0 e	22.3	0.0
2.4	748.4	769.3	-164.9	GCBW	11.1	0.6 e	29.0	0.0
3.3	758.1	779.1	-166.6	GCBW	9.6	0.3 e	23.6	0.0
4.2	768.0	788.9	-168.4	GCBW	12.3	0.4 e	28.7	0.0

upstream east-west coordinate (m) X	upstream north-south coordinate (m) Y	upstream length coordinate (m) L	upstream surface elevation (m) Z	section bed material M	upstream bed width (m) W	upstream bed depth (m) D	section bed volume (m^3) V_B	section sideslope volume (m^3) V_S
5.0	777.4	798.4	-171.7	GCBW	10.5	0.4 e	36.4	0.0
6.3	792.1	813.1	-174.4	GCBW	8.0	0.4 e	22.9	0.0
7.1	801.6	822.7	-177.4	GCB	10.0	0.4 e	27.1	0.0
8.0	811.4	832.6	-178.7	GCBW	10.5	0.4 e	26.8	0.0
8.8	821.2	842.4	-180.7	GCB	10.0	0.4 e	26.3	16.5
9.7	831.5	852.8	-182.3	GCB	9.0	0.4 e	33.9	0.0
10.5	840.9	862.2	-183.5	GCB	18.0	0.4 e	46.4	84.2
11.4	850.8	872.1	-184.6	GCB	17.0	0.4 e	55.7	0.0
12.4	862.2	883.6	-185.8	GCBW	19.5	0.4 e	82.7	0.0
13.6	875.6	897.0	-187.4	GCBW	11.0	0.9 e	32.0	0.0
		907.0	-189.2		12.0			

WT

Old-growth Forest

upstream east-west coordinate (m) X	upstream north-south coordinate (m) Y	upstream length coordinate (m) L	upstream surface elevation (m) Z	section bed material M	upstream bed width (m) W	upstream bed depth (m) D	section bed volume (m^3) V_B	section sideslope volume (m^3) V_S
0.0	0.0	0.0	0.0	GCB	2.0	0.3 e	3.9	0.0
4.9	-1.8	5.2	-1.5	BR	2.4	0.7	0.0	0.0
9.7	-3.5	10.4	-4.1	GCBW	1.0	0.7 e	13.2	0.0
15.1	-5.5	16.1	-5.8	GCBW	3.4	2.2 e	55.5	0.0
24.3	-8.9	25.9	-10.2	GCBW	3.0	3.2 e	22.1	0.0
29.3	-10.7	31.2	-14.6	CB	2.0	1.7 e	8.1	0.0
35.3	-12.9	37.6	-16.8	BR	2.0	0.2	0.0	0.0
46.0	-16.8	49.0	-22.0	BR	1.5	0.0	0.0	0.0
52.8	-19.2	56.2	-24.5	GCBW	3.0	0.0 e	114.6	0.0
71.8	-22.6	75.5	-28.3	GCW	9.5	2.4 e	87.0	0.0
79.1	-23.9	82.9	-32.0	GCBW	11.0	1.0 e	46.2	0.0
89.7	-25.7	93.6	-36.2	GCBW	8.0	0.3 e	1.6	0.0
90.5	-25.9	94.5	-38.0	GCBW	8.0	0.4 e	19.0	0.0
101.8	-27.9	105.9	-41.4	GCBW	4.5	0.4 e	6.4	0.0
110.4	-29.4	114.6	-43.1	GCBW	5.0	0.1 e	43.0	72.0
124.5	-37.5	131.0	-46.2	GCB	2.5	2.3 e	85.4	0.0
134.0	-43.0	142.0	-48.2	GCB	5.0	3.8 e	853.6	0.0
157.7	-56.7	169.3	-52.5	GCB	10.0	8.2 e	372.6	0.0
168.4	-61.7	181.1	-60.5	CBW	5.0	4.0 e	127.8	0.0
177.3	-65.8	190.9	-63.3	GCBW	4.0	4.7 e	157.5	0.0
188.6	-71.1	203.4	-68.7	BW	5.0	3.7 e	63.8	0.0
195.5	-74.3	211.0	-73.4	GCBW	4.0	1.7 e	57.2	0.0
209.0	-80.6	225.9	-79.4	BW	4.5	1.0 e	10.6	0.0
212.8	-82.8	230.3	-81.6	CBW	4.6	0.6 e	7.0	0.0
216.8	-85.2	235.0	-83.5	CB	4.2	0.5 e	5.0	0.0
220.5	-87.3	239.2	-86.2	GCBW	3.8	0.4 e	4.6	0.0
224.6	-89.6	244.0	-87.8	LJ	3.4	0.4 e	3.9	0.0
228.6	-92.0	248.6	-89.7	GCB	3.0	0.4 e	3.9	0.0
232.4	-94.6	253.2	-91.6	GCB	3.3	0.4 e	2.2	0.0
236.3	-97.3	258.0	-93.1	BR	3.7	0.0	0.0	0.0
240.3	-100.1	262.8	-94.3	GCB	4.0	0.0 e	0.0	0.0
244.2	-102.9	267.6	-95.8	BR	4.4	0.0	0.0	0.0
248.0	-105.5	272.2	-97.8	LJ	4.7	0.0 e	2.7	0.0
251.7	-108.1	276.7	-99.9	LJ	4.5	0.4 e	5.5	0.0
255.4	-110.7	281.3	-101.8	GCB	4.4	0.4 e	5.1	0.0
259.1	-113.3	285.8	-104.1	LJ	4.2	0.4 e	5.1	0.0

upstream east-west coordinate (m) X	upstream north-south coordinate (m) Y	upstream length coordinate (m) L	upstream surface elevation (m) Z	section bed material M	upstream bed width (m) W	upstream bed depth (m) D	section bed volume (m^3) V_B	section sideslope volume (m^3) V_S
262.9	-115.9	290.4	-106.1	LJ	4.1	0.4 e	4.7	0.0
266.4	-118.4	294.7	-108.5	GCB	3.9	0.4 e	5.2	0.0
271.3	-119.3	299.6	-109.5	GCB	4.1	0.4 e	2.7	0.0
276.0	-120.1	304.5	-110.7	BR	4.3	0.0	0.0	0.0
280.8	-121.0	309.3	-112.1	GCB	4.5	0.0 e	2.9	0.0
285.4	-121.8	314.0	-113.8	GCB	4.7	0.4 e	6.2	0.0
290.1	-122.6	318.8	-115.2	GCB	4.9	0.4 e	8.2	0.0
294.5	-123.4	323.3	-115.8	GCB	5.1	0.7 e	6.6	0.0
298.6	-124.1	327.4	-117.6	LJ	5.3	0.2 e	5.4	0.0
303.3	-124.9	332.2	-120.3	LJ	5.6	0.4 e	5.2	0.0
306.7	-125.5	335.6	-121.1	GCB	5.8	0.4 e	6.8	0.0
311.1	-126.3	340.1	-121.4	GCB	6.0	0.4 e	12.9	0.0
314.2	-128.8	344.1	-121.7	GCB	5.5	1.3 e	23.6	0.0
317.7	-131.5	348.5	-122.6	LJ	5.0	1.7 e	28.1	0.0
320.8	-133.9	352.4	-122.9	LJ	4.5	2.7 e	26.2	0.0
323.7	-136.2	356.1	-124.5	LJ	4.0	2.3 e	16.3	0.0
326.7	-138.5	359.9	-126.9	LJ	3.5	1.1 e	3.8	0.0
329.5	-139.3	362.8	-128.9	BR	3.9	0.0	0.0	0.0
332.7	-140.1	366.1	-130.1	GCB	4.3	0.0 e	4.7	0.0
336.1	-141.0	369.6	-130.2	GCB	4.8	0.9 e	14.1	0.0
339.9	-142.1	373.5	-131.0	GCB	5.2	1.3 e	18.3	0.0
343.2	-142.9	377.0	-131.6	GCB	5.6	1.7 e	20.7	0.0
347.0	-144.0	380.9	-133.3	CB	5.5	1.2 e	17.9	0.0
351.1	-145.1	385.1	-134.5	GC	5.5	1.2 e	24.6	0.0
355.2	-146.2	389.4	-134.9	GC	5.4	2.0 e	12.5	0.0
356.8	-146.6	391.0	-135.1	GCW	5.4	2.3 e	7.4	0.0
358.0	-146.9	392.3	-136.8	GC	5.4	1.0 e	20.6	0.0
362.4	-148.1	396.9	-137.6	GCB	5.3	1.5 e	20.3	0.0
364.7	-151.4	400.9	-138.9	GCB	5.3	1.4 e	20.6	0.0
367.0	-154.6	404.8	-139.9	GC	5.3	1.6 e	21.2	0.0
369.3	-157.9	408.8	-141.2	LJ	5.4	1.4 e	2.3	0.0
369.8	-158.6	409.7	-142.9	BR	5.4	0.0	0.0	0.0
371.1	-160.5	412.0	-142.7	GC	5.4	0.0 e	0.0	0.0
373.3	-163.6	415.8	-144.2	BR	5.4	0.0	0.0	0.0
374.4	-165.7	418.2	-145.0	BR	5.3	0.0	0.0	0.0
374.9	-166.7	419.3	-146.3	BR	5.3	0.0	0.0	0.0
376.9	-170.3	423.4	-146.3	GCB	5.2	0.0 e	2.2	0.0
378.8	-174.0	427.6	-146.9	GCB	5.1	0.3 e	2.1	0.0
380.7	-177.6	431.6	-148.1	BR	5.0	0.0	0.0	0.0
382.6	-181.1	435.6	-149.0	GCB	4.9	0.0 e	0.0	0.0
384.0	-185.3	440.0	-149.8	BR	4.9	0.0	0.0	0.0
385.5	-189.9	444.9	-151.3	BR	4.9	0.0	0.0	0.0
386.6	-193.5	448.6	-152.8	BR	4.8	0.0	0.0	0.0
387.9	-197.6	452.9	-154.4	BR	4.8	0.0	0.0	0.0
389.3	-201.8	457.4	-155.3	BR	4.8	0.0	0.0	0.0
392.3	-205.0	461.8	-156.1	BR	4.7	0.0	0.0	0.0
395.4	-208.3	466.3	-156.5	GCB	4.6	0.0 e	2.8	0.0
398.5	-211.6	470.8	-157.3	GCB	4.6	0.4 e	5.4	0.0
401.5	-214.8	475.2	-158.5	GCB	4.5	0.4 e	2.7	0.0
404.6	-218.1	479.7	-158.7	BR	4.4	0.0	0.0	0.0
408.4	-220.1	484.0	-160.0	GCB	4.4	0.0 e	0.6	0.0
412.3	-222.1	488.5	-160.9	GCB	5.3	0.1 e	3.0	0.0
416.4	-224.1	493.0	-161.8	GCB	5.8	0.3 e	8.0	0.0
420.4	-226.2	497.5	-162.5	GCB	6.2	0.6 e	20.0	0.0
424.4	-228.3	502.0	-162.7	GC	6.7	1.4 e	29.7	0.0
427.2	-231.3	506.2	-163.3	LJ	6.5	1.8 e	19.7	0.0

upstream east-west coordinate (m) X	upstream north-south coordinate (m) Y	upstream length coordinate (m) L	upstream surface elevation (m) Z	section bed material M	upstream bed width (m) W	upstream bed depth (m) D	section bed volume (m^3) V_B	section sideslope volume (m^3) V_S
429.6	-234.0	509.8	-165.2	GCB	6.3	0.7 e	12.4	0.0
432.4	-237.1	513.9	-166.1	GCB	6.2	0.7 e	9.7	0.0
434.5	-239.5	517.1	-166.8	GCB	6.0	0.8 e	15.0	0.0
437.2	-242.4	521.1	-167.3	LJ	5.8	1.2 e	11.3	0.0
440.1	-244.8	524.8	-169.0	GCB	6.0	0.4 e	5.4	0.0
443.2	-247.5	528.9	-170.0	GCB	6.2	0.3 e	6.6	0.0
446.3	-250.1	533.0	-170.7	GCB	6.5	0.5 e	6.1	0.0
449.4	-252.6	537.0	-171.9	GCB	6.7	0.2 e	6.6	0.0
452.5	-255.2	541.0	-172.5	GCB	6.9	0.5 e	7.9	0.0
454.6	-258.2	544.7	-173.5	GCB	6.9	0.4 e	14.0	0.0
456.9	-261.4	548.6	-173.6	GCB	6.9	1.2 e	22.6	0.0
459.1	-264.4	552.4	-174.2	LJ	6.9	1.5 e	22.3	0.0
461.4	-267.5	556.2	-175.4	LJ	6.9	1.1 e	17.8	0.0
463.5	-270.4	559.8	-176.3	GCB	6.9	1.1 e	22.9	0.0
466.7	-273.4	564.2	-177.2	GCB	6.9	1.2 e	14.6	0.0
469.7	-276.2	568.3	-178.9	GCB	6.1	0.4 e	5.4	0.0
472.5	-278.8	572.1	-179.9	B	5.8	0.3 e	6.4	0.0
476.1	-282.2	577.1	-180.9	GCB	5.4	0.4 e	2.8	0.0
479.3	-285.1	581.4	-182.3	BR	5.0	0.0	0.0	0.0
482.5	-287.7	585.5	-183.0	BR	4.7	0.0	0.0	0.0
485.6	-290.1	589.4	-184.5	BR	4.5	0.0	0.0	0.0
488.8	-292.6	593.5	-185.2	BR	4.2	0.0	0.0	0.0
492.0	-295.1	597.6	-185.7	BR	4.0	0.0	0.0	0.0
494.8	-297.3	601.1	-187.9	BR	3.7	0.0	0.0	0.0
498.1	-299.6	605.1	-188.0	BR	4.5	0.0	0.0	0.0
501.4	-302.1	609.2	-188.3	GCB	5.3	0.0 e	2.2	0.0
504.6	-304.4	613.2	-188.7	GCB	6.2	0.3 e	5.7	0.0
507.6	-306.6	616.9	-190.1	GCB	7.0	0.4 e	7.7	0.0
510.8	-308.9	620.8	-190.4	GCB	7.8	0.4 e	5.8	0.0
514.5	-311.5	625.4	-190.8	GCB	7.9	0.1 e	4.9	0.0
518.3	-314.1	630.0	-191.3	GCB	8.0	0.3 e	7.7	0.0
522.1	-316.8	634.6	-192.1	GCB	8.0	0.3 e	7.2	0.0
525.8	-319.4	639.2	-192.8	GCB	8.1	0.3 e	3.4	0.0
529.5	-322.0	643.6	-193.8	BR	8.2	0.0	0.0	0.0
533.6	-323.1	647.9	-194.2	GCB	8.2	0.0 e	2.2	0.0
537.8	-324.2	652.3	-194.7	GCB	7.7	0.2 e	5.2	0.0
541.9	-325.3	656.6	-195.3	GCB	7.1	0.3 e	6.8	0.0
546.0	-326.4	660.8	-196.5	GCB	6.6	0.4 e	3.6	0.0
550.2	-327.5	665.1	-197.1	BR	6.0	0.0	0.0	0.0
553.3	-330.7	669.6	-198.0	GCB	5.0	0.0 e	3.6	0.0
556.6	-334.0	674.2	-198.8	GCB	6.3	0.4 e	18.6	0.0
563.1	-340.4	683.3	-200.0	GCB	9.0	0.4 e	25.0	0.0
569.6	-347.0	692.6	-200.3	GCB	7.5	0.6 e	61.2	0.0
576.8	-354.2	702.8	-200.8	GCB	10.0	1.4 e	84.1	0.0
584.4	-359.1	711.8	-201.9	GCB	9.5	1.4 e	67.3	0.0
591.8	-363.9	720.7	-203.6	GCBW	10.5	0.9 e	52.7	0.0
599.4	-368.8	729.7	-204.8	GCBW	10.5	0.8 e	40.8	0.0
608.7	-374.9	740.8	-206.9	GCBW	14.0	0.1 e	18.5	0.0
615.9	-374.6	748.0	-208.4	GCBW	15.0	0.4 e	36.8	0.0
625.1	-374.3	757.2	-209.7	GCBW	15.0	0.4 e	26.6	0.0
633.4	-374.0	765.5	-211.0	GCB	9.0	0.4 e	9.0	20.0
637.0	-373.9	769.1	-211.6	GCB	10.0	0.4 e	29.3	0.0
647.3	-375.7	779.6	-212.2	GCB	11.0	0.4 e	31.5	0.0
656.8	-377.4	789.3	-212.8	GCB	12.0	0.4 e	40.1	12.7
666.3	-379.1	798.9	-214.0	GCB	15.0	0.5 e	32.9	0.0
673.2	-384.9	807.9	-215.1	GCB	8.0	0.5 e	16.6	12.5

upstream east-west coordinate (m) X	upstream north-south coordinate (m) Y	upstream length coordinate (m) L	upstream surface elevation (m) Z	section bed material M	upstream bed width (m) W	upstream bed depth (m) D	section bed volume (m^3) V_B	section sideslope volume (m^3) V_S
680.2	-390.7	817.0	-216.5	GCB	6.2	0.3 e	10.0	0.0
687.1	-396.5	826.0	-217.7	GCB	8.1	0.2 e	7.7	46.6
694.9	-393.7	834.4	-218.8	GCBW	8.8	0.1 e	12.2	51.0
703.2	-390.7	843.2	-220.1	GCBW	6.8	0.4 e	13.8	0.0
713.4	-387.0	854.0	-221.3	GCBW	7.3	0.1 e	1.4	0.0
717.5	-385.5	858.3	-222.0	BR	5.5	0.0	0.0	0.0
725.5	-388.9	867.1	-223.1	GCB	5.4	0.0 e	6.2	0.0
733.7	-392.3	875.9	-224.2	GCB	5.2	0.4 e	14.2	0.0
741.7	-395.7	884.6	-225.4	GCB	7.0	0.4 e	18.7	4.4
750.6	-399.5	894.3	-226.3	GCB	7.5	0.4 e	10.8	0.0
756.6	-405.6	902.8	-227.2	GCB	9.5	0.1 e	9.5	5.5
762.6	-411.6	911.3	-228.5	GCB	6.0	0.4 e	19.9	0.0
768.7	-417.6	919.9	-229.6	GCB	11.5	0.4 e	14.6	52.9
771.7	-420.6	924.2	-229.8	GCB	14.0	0.4 e	33.1	52.9
780.7	-421.4	933.2	-232.1	GCB	13.5	0.4 e	30.4	0.0
789.8	-422.2	942.3	-233.7	GCB	11.4	0.4 e	26.6	0.0
799.1	-423.0	951.7	-234.8	GCB	10.0	0.4 e	25.0	0.0
809.7	-424.0	962.3	-237.9	GCB	7.6	0.4 e	16.0	0.0
817.2	-424.6	969.8	-238.7	GCB	8.5	0.4 e	25.3	36.4
826.4	-425.4	979.0	-239.6	GCB	12.0	0.4 e	32.1	36.4
835.6	-426.2	988.3	-240.1	GC	13.9	0.4 e	30.3	20.7
843.0	-426.9	995.7	-241.3	GC	16.8	0.4 e	37.5	62.4
851.0	-423.6	1004.4	-242.3	GC	15.8	0.4 e	37.1	62.4
859.1	-420.4	1013.1	-243.0	GC	15.9	0.4 e	35.4	44.1
867.2	-417.1	1021.8	-243.6	GC	14.7	0.4 e	39.0	44.1
878.5	-417.5	1033.1	-244.0	GC	11.2	0.4 e	30.8	5.8
887.8	-417.8	1042.5	-244.8	GC	13.5	0.4 e	12.6	0.0
891.5	-418.0	1046.2	-245.0	GC	12.1	0.4 e	29.0	546.9
897.8	-414.3	1053.4	-245.6	GC	17.8	0.4 e	43.2	0.0
906.2	-409.5	1063.1	-246.6	GC	15.8	0.4 e	47.1	0.0
917.0	-403.3	1075.6	-247.2	GC	11.4	0.4 e	47.6	225.7
926.5	-406.2	1085.6	-247.9	GC	10.1	0.9 e	90.5	0.0
936.1	-409.1	1095.5	-248.4	GCW	12.0	1.5 e	190.7	0.0
945.6	-412.0	1105.5	-249.0	GCW	19.1	2.1 e	245.9	40.9
955.2	-414.9	1115.5	-249.4	LJ	10.9	2.9 e	106.3	0.0
964.7	-417.8	1125.5	-250.4	LJ	0.0	3.1 e	0.0	0.0
968.8	-419.1	1129.8	-251.6	TER		2.4 e	0.0	0.0
972.8	-420.3	1133.9	-254.5	BR		0.0	0.0	0.0
		1139.4	-255.1					

ET

Old-growth Forest

upstream east-west coordinate (m) X	upstream north-south coordinate (m) Y	upstream length coordinate (m) L	upstream surface elevation (m) Z	section bed material M	upstream bed width (m) W	upstream bed depth (m) D	section bed volume (m^3) V_B	section sideslope volume (m^3) V_S
0.0	0.0	0.0	0.0	BR	2.9	0.0	0.0	0.0
1.7	-1.0	2.0	-0.3	GCB	2.9	0.0 e	1.3	0.0
6.0	-3.5	6.9	-0.9	GCB	3.2	0.3 e	1.2	0.0
10.2	-5.9	11.8	-2.1	BR	2.3	0.0	0.0	0.0
12.8	-7.4	14.7	-2.7	BR	2.0	0.0	0.0	0.0
19.2	-11.1	22.2	-5.5	GCB	4.0	0.0 e	3.8	0.0
26.9	-15.5	31.1	-7.9	GCB	4.0	0.3 e	16.3	0.0
34.6	-20.0	40.0	-10.1	GCBW	5.3	0.8 e	13.7	0.0

upstream east-west coordinate (m) X	upstream north-south coordinate (m) Y	upstream length coordinate (m) L	upstream surface elevation (m) Z	section bed material M	upstream bed width (m) W	upstream bed depth (m) D	section bed volume (m^3) V_B	section sideslope volume (m^3) V_S
37.7	-21.8	43.6	-10.9	GCBW	6.0	1.2 e	31.0	0.0
46.0	-24.0	52.1	-14.0	GCBW	5.7	0.7 e	30.8	0.0
54.5	-26.3	60.9	-16.1	GCBW	5.0	1.3 e	24.7	0.0
59.5	-27.6	66.1	-17.9	LJ	7.0	1.1 e	6.1	0.0
62.4	-28.4	69.1	-20.0	BR	2.5	0.0	0.0	0.0
70.6	-30.6	77.6	-23.2	BR	0.0	0.0	0.0	0.0
71.8	-30.9	78.8	-23.8	GCBW	4.0	0.0 e	1.8	0.0
78.0	-32.6	85.2	-26.0	GCBW	2.2	0.3 e	1.0	0.0
81.0	-37.8	91.3	-28.6	BR	0.5	0.0	0.0	0.0
82.3	-40.1	93.9	-29.6	BR	1.0	0.0	0.0	0.0
86.7	-47.7	102.7	-32.9	GCBW	3.0	0.0 e	0.0	0.0
88.1	-50.1	105.5	-33.5	BR	0.0	0.0	0.0	2.3
93.2	-58.8	115.6	-38.5	GCB	0.0	0.0 e	9.2	0.0
96.4	-64.5	122.2	-38.7	GCB	5.5	1.1 e	26.7	0.0
99.5	-73.0	131.2	-40.8	GCBW	3.5	0.8 e	18.7	0.0
102.0	-79.9	138.5	-42.1	LJ	5.5	0.9 e	9.7	0.0
103.3	-83.4	142.3	-44.8	GCB	6.5	0.4 e	11.6	0.0
105.5	-89.5	148.7	-45.6	GCB	7.0	0.4 e	10.3	0.0
107.7	-95.6	155.2	-46.0	LJ	7.5	0.3 e	3.6	0.0
108.6	-97.9	157.7	-47.3	GCB	6.0	0.4 e	6.3	0.0
110.8	-104.0	164.1	-48.0	GCB	8.5	0.0 e	7.9	41.7
111.6	-113.0	173.1	-50.0	GCBW	5.0	0.4 e	17.4	0.0
112.4	-122.1	182.3	-51.1	GCB	9.0	0.4 e	11.3	24.3
113.2	-131.0	191.3	-53.2	GCB	5.5	0.1 e	0.8	0.0
113.7	-137.4	197.6	-54.5	BR	3.0	0.0	0.0	0.0
114.3	-144.5	204.8	-56.1	BR	3.0	0.0	0.0	15.1
114.7	-149.1	209.4	-56.6	BR	3.0	0.0	0.0	0.0
115.5	-158.2	218.6	-57.8	GCB	3.0	0.0 e	9.3	48.8
117.1	-167.1	227.6	-58.7	GCB	4.3	0.8 e	38.2	0.0
118.7	-176.1	236.7	-59.5	GCB	5.5	1.8 e	80.8	0.0
120.4	-185.8	246.6	-60.7	GCB	6.3	2.4 e	55.7	0.0
121.8	-193.6	254.5	-62.8	GCB	3.8	1.8 e	46.8	0.0
123.3	-202.4	263.5	-64.5	GCB	5.1	1.8 e	40.8	0.0
124.8	-210.9	272.1	-67.4	GCB	8.2	0.5 e	19.5	0.0
126.4	-219.7	281.0	-69.1	GCB	5.0	0.5 e	10.9	0.0
127.9	-228.5	289.9	-70.9	GCB	3.5	0.3 e	0.7	0.0
128.2	-230.1	291.6	-71.6	BR	3.5	0.0	0.0	0.0
129.5	-237.2	298.8	-72.8	GCB	3.4	0.0 e	12.4	0.0
131.0	-246.1	307.8	-73.5	GCB	5.0	0.9 e	76.8	46.2
132.9	-256.8	318.7	-74.4	LJ	8.6	2.1 e	48.3	0.0
133.7	-261.1	323.0	-75.9	GCB	10.8	1.4 e	153.3	0.0
135.7	-272.8	334.9	-76.4	GCB	6.8	3.1 e	21.9	0.0
136.0	-274.4	336.6	-77.2	GCB	6.6	2.7 e	63.6	18.8
139.9	-279.9	343.3	-79.3	GCB	6.0	1.8 e	74.8	0.0
145.9	-288.5	353.8	-80.7	GCB	4.3	2.4 e	55.8	0.0
149.9	-294.3	360.8	-81.6	GCB	4.9	2.8 e	88.7	0.0
154.9	-301.5	369.6	-82.4	GCB	4.5	3.7 e	101.4	0.0
158.9	-309.9	378.9	-83.8	GCB	4.0	4.0 e	142.3	0.0
162.9	-318.5	388.4	-84.6	GCB	6.0	5.0 e	142.8	0.0
165.4	-323.8	394.2	-84.6	LJ	7.2	6.1 e	97.3	0.0
166.8	-326.9	397.7	-85.7	GC	7.0	5.7 e	301.5	0.0
170.8	-335.5	407.2	-86.3	GC	8.2	6.9 e	471.1	0.0
174.8	-344.1	416.6	-87.0	GC	12.0	7.9 e	204.2	0.0
176.4	-347.5	420.4	-87.6	LJ	8.6	8.0 e	409.6	0.0
180.1	-355.4	429.1	-89.7	GC	9.5	7.5 e	358.7	0.0
186.5	-357.8	436.0	-91.2	GC	11.6	7.4 e	205.9	0.0

upstream east-west coordinate (m) X	upstream north-south coordinate (m) Y	upstream length coordinate (m) L	upstream surface elevation (m) Z	section bed material M	upstream bed width (m) W	upstream bed depth (m) D	section bed volume (m^3) V_B	section sideslope volume (m^3) V_S
190.3	-359.1	439.9	-91.6	GC	9.0	7.7 e	172.6	0.0
195.1	-360.9	445.1	-94.7	GCB	6.0	5.6 e	190.1	0.0
204.5	-364.3	455.0	-95.6	GCB	3.5	6.6 e	140.8	0.0
213.8	-367.7	465.0	-96.4	GCB	2.5	7.6 e	174.6	0.0
222.9	-371.9	474.9	-97.4	GCB	4.0	8.5 e	241.0	21.0
231.9	-376.1	484.9	-98.1	GCBW	4.0	9.6 e	253.7	0.0
236.9	-384.7	494.9	-98.9	GC	3.5	10.8 e	362.7	0.0
241.8	-393.3	504.8	-100.1	GCBW	6.4	11.4 e	500.4	0.0
246.8	-401.9	514.7	-101.6	GCB	6.7	11.8 e	415.7	0.0
253.8	-409.0	524.7	-102.4	GC	3.5	12.8 e	333.1	0.0
260.9	-416.0	534.6	-103.2	GCBW	4.0	13.9 e	402.7	0.0
267.9	-423.0	544.6	-104.3	GCB	4.5	14.7 e	433.3	0.0
275.0	-430.1	554.6	-104.9	GCB	4.0	16.0 e	230.4	0.0
		564.6	-105.4	GC	5.0			

HBC

Old-growth Forest

upstream east-west coordinate (m) X	upstream north-south coordinate (m) Y	upstream length coordinate (m) L	upstream surface elevation (m) Z	section bed material M	upstream bed width (m) W	upstream bed depth (m) D	section bed volume (m^3) V_B	section sideslope volume (m^3) V_S
0.0	0.0	0.0	0.0	BR		0.0	0.0	0.0
17.0	-20.3	26.4	-16.4	BR		0.0	0.0	0.0
29.6	-35.3	46.1	-25.6	BR		0.0	0.0	0.0
32.8	-39.1	51.1	-29.9	BR		0.0	0.0	0.0
38.1	-45.3	59.2	-32.8	BR		0.0	0.0	0.0
39.1	-46.6	60.8	-34.7	BR	6.0	0.0	0.0	0.0
44.6	-54.5	70.5	-37.3	GCBW	7.0	0.0 e	138.7	0.0
57.8	-73.3	93.4	-42.3	LJ	7.0	2.6 e	464.5	99.0
128.5	-106.2	171.4	-68.3	LJ	4.7	2.5 e	189.1	0.0
153.5	-117.9	199.0	-78.1	CBW	4.7	1.9 e	137.0	0.0
178.7	-129.7	226.8	-87.7	GCBW	4.0	1.5 e	8.1	0.0
182.4	-131.4	230.9	-89.0	BR	3.9	0.0	0.0	0.0
187.7	-133.9	236.7	-91.1	LJ	4.4	0.0 e	9.5	0.0
199.2	-139.2	249.5	-95.6	LJ	5.1	0.4 e	12.3	0.0
206.6	-145.4	259.1	-98.3	LJ	4.5	0.5 e	8.4	0.0
210.4	-148.6	264.1	-101.6	LJ	7.2	0.4 e	8.2	0.0
214.4	-151.9	269.2	-104.7	GCBW	4.7	0.4 e	4.1	0.0
216.7	-153.9	272.2	-104.9	GCBW	5.5	0.4 e	6.0	0.0
220.4	-157.0	277.1	-106.1	GCBW	3.8	0.4 e	4.7	0.0
227.8	-163.2	286.8	-108.4	GCBW	9.1	0.4 e	7.3	0.0
231.2	-169.1	293.6	-110.3	CBW	6.0	0.3 e	3.9	0.0
234.1	-174.1	299.4	-111.9	BR	5.4	0.0	0.0	0.0
234.6	-174.9	300.3	-113.0	GCB	4.4	0.0 e	0.0	0.0
238.8	-182.3	308.8	-113.7	GCBW	8.0	0.2 e	0.6	0.0
239.3	-183.1	309.7	-114.1	BR	8.0	0.0	0.0	0.0
242.7	-189.0	316.6	-117.1	BR	3.8	0.0	0.0	0.0
247.5	-197.4	326.2	-119.7	BR	2.7	0.0	0.0	0.0
250.8	-204.4	334.0	-121.7	BR	4.6	0.0	0.0	0.0
254.9	-213.2	343.7	-124.0	BR	3.8	0.0	0.0	0.0
259.1	-222.1	353.5	-126.1	BR	3.2	0.0	0.0	12.3
263.2	-231.0	363.4	-127.6	BR	4.7	0.0	0.0	0.0
267.3	-239.8	373.1	-130.1	BR	5.2	0.0	0.0	0.0
271.5	-248.7	382.8	-132.3	BR		0.0	0.0	0.0

upstream east-west coordinate (m) X	upstream north-south coordinate (m) Y	upstream length coordinate (m) L	upstream surface elevation (m) Z	section bed material M	upstream bed width (m) W	upstream bed depth (m) D	section bed volume (m^3) V_B	section sideslope volume (m^3) V_S
275.9	-258.2	393.4	-135.5	GCBW	4.6	0.0 e	5.0	0.0
277.6	-261.8	397.4	-135.4	GCB	7.0	0.9 e	29.6	0.0
281.7	-270.7	407.1	-137.6	GCB	7.0	0.6 e	4.3	0.0
283.2	-272.8	409.7	-139.1	GCB	7.2	0.4 e	45.2	0.0
288.8	-280.8	419.5	-141.3	GCB	5.4	0.1 e	34.8	0.0
294.5	-289.0	429.4	-142.1	GCB	5.6	1.9 e	26.6	0.0
298.7	-295.5	437.2	-144.2	GCBW		1.8 e	8.8	0.0
301.4	-299.5	442.0	-145.5	GCBW	9.1	1.8 e	7.4	0.0
302.5	-301.2	444.1	-147.8	BR		0.0	0.0	0.0
304.1	-303.7	447.0	-148.2	CB	4.5	0.0 e	21.4	0.0
309.5	-312.1	457.0	-149.1	GCB	9.8	1.9 e	95.6	0.0
314.6	-319.9	466.3	-152.8	GCBW	13.1	0.8 e	38.3	0.0
316.5	-326.4	473.0	-154.7	GCBW	14.2	0.9 e	53.2	0.0
318.6	-333.7	480.6	-157.2	GCBW	10.9	0.5 e	30.5	0.0
321.2	-343.0	490.3	-159.6	GCBW	4.0	0.8 e	35.0	0.0
323.9	-352.5	500.2	-161.3	GCBW	4.6	0.9 e	32.0	0.0
322.6	-357.3	505.2	-161.4	GCBW	7.1	1.7 e	91.1	0.0
319.8	-366.8	515.1	-162.5	GCBW	7.0	2.3 e	130.6	0.0
317.1	-376.3	525.0	-164.3	GCBW	11.9	2.2 e	146.2	0.0
314.4	-385.7	534.8	-166.3	GCBW	13.1	1.9 e	94.4	0.0
311.7	-395.1	544.5	-168.6	LJ	7.3	1.4 e	31.4	0.0
309.0	-404.4	554.2	-170.8	GCBW	6.9	0.8 e	21.1	0.0
306.4	-413.7	563.9	-173.3	BR	10.7	0.0	0.0	0.0
312.0	-421.7	573.7	-175.4	BR		0.0	0.0	0.0
315.4	-426.6	579.6	-178.1	BR		0.0	0.0	0.0
319.5	-432.5	586.9	-180.0	BR	3.7	0.0	0.0	0.0
324.5	-439.6	595.5	-182.4	GCBW	5.0	0.0 e	100.5	0.0
328.5	-445.3	602.5	-183.5	LJ	8.4	2.2 e	72.3	0.0
334.2	-453.5	612.4	-184.5		12.4	6.0 e		

SP

Old-growth Forest

upstream east-west coordinate (m) X	upstream north-south coordinate (m) Y	upstream length coordinate (m) L	upstream surface elevation (m) Z	section bed material M	upstream bed width (m) W	upstream bed depth (m) D	section bed volume (m^3) V_B	section sideslope volume (m^3) V_S
0.0	0.0	0.0	0.0	GCBW	9.0	5.3 e	282.5	0.0
-0.5	-9.3	9.3	-3.7	GCBW	9.0	4.9 e	252.1	0.0
-1.0	-18.6	18.7	-7.2	GCBW	8.0	4.6 e	206.0	0.0
-1.4	-27.6	27.7	-11.6	GCBW	9.0	3.5 e	158.3	0.0
-1.9	-36.7	36.7	-15.8	GCBW	9.0	2.4 e	100.7	0.0
-2.4	-45.8	45.8	-19.9	GCBW	8.0	1.5 e	64.8	0.0
-2.9	-55.0	55.1	-23.7	GCBW	9.0	1.0 e	26.7	0.0
-3.4	-64.1	64.2	-27.9	BR	9.0	0.0	0.0	0.0
-3.8	-73.1	73.2	-32.2	BR	8.3	0.0	0.0	90.0
-4.3	-82.3	82.5	-36.0	BR	3.3	0.0	0.0	120.0
-4.8	-92.0	92.1	-38.6	BR	2.0	0.0	0.0	108.0
-7.2	-98.4	99.0	-44.4	GCBW	5.0	0.0 e	3.6	67.5
-10.6	-107.8	109.0	-48.9	GCBW	1.5	0.4 e	2.5	60.0
-13.2	-114.9	116.5	-51.8	BR	4.5	0.0	0.0	0.0
-15.6	-121.5	123.6	-57.3	GCB	4.5	0.0 e	5.3	0.0
-16.6	-124.3	126.6	-56.9	GCB	4.5	1.2 e	23.6	0.0
-19.8	-133.2	135.9	-60.4	GCB	5.5	0.4 e	8.6	0.0
-23.1	-142.2	145.5	-63.3	GCB	4.5	0.2 e	2.7	0.0

upstream east-west coordinate (m) X	upstream north-south coordinate (m) Y	upstream length coordinate (m) L	upstream surface elevation (m) Z	section bed material M	upstream bed width (m) W	upstream bed depth (m) D	section bed volume (m^3) V_B	section sideslope volume (m^3) V_S
-26.4	-151.2	155.1	-66.2	BR	5.0	0.0	0.0	0.0
-29.7	-160.2	164.7	-68.9	BR	5.0	0.0	0.0	0.0
-33.8	-171.5	176.7	-76.1	GCB	5.0	0.0 e	14.4	0.0
-35.8	-177.1	182.7	-76.0	GCB	5.0	1.4 e	58.2	0.0
-28.7	-183.1	191.9	-79.8	GCB	18.0	0.4 e	52.3	0.0
-21.1	-189.4	201.9	-81.1	GCBW	18.0	0.5 e	170.9	0.0
-13.5	-195.9	211.9	-81.4	GCBW	17.0	2.5 e	97.8	0.0
-10.6	-198.3	215.7	-82.6	GCBW	17.0	2.1 e	50.1	0.0
-7.8	-200.7	219.3	-87.4	GCBW	16.0	0.4 e	42.3	0.0
-0.2	-207.0	229.2	-88.7	GCBW	16.0	0.4 e	36.0	0.0
7.2	-213.2	238.9	-91.4	GCB	12.0	0.4 e	20.0	0.0
14.0	-218.9	247.7	-96.1	GCB	5.0	0.4 e	17.0	80.0
21.5	-225.2	257.5	-98.0	GCB	8.0	0.4 e	21.1	20.0
29.1	-231.6	267.4	-99.4	GCB	8.0	0.4 e	17.9	0.0
35.1	-236.6	275.3	-100.8	GCB	9.0	0.4 e	23.6	0.0
42.0	-243.6	285.1	-102.7	GCB	9.0	0.4 e	26.5	0.0
49.1	-250.6	295.0	-103.8	GCB	11.0	0.4 e	31.7	0.0
56.1	-257.6	304.9	-105.2	GCBW	13.0	0.4 e	30.8	0.0
62.3	-263.9	313.8	-106.7	GCBW	13.0	0.4 e	54.4	0.0
70.1	-271.6	324.8	-107.8	GCBW	9.0	1.0 e	60.5	0.0
77.1	-278.6	334.6	-109.5	GCBW	6.0	1.5 e	26.4	545.0
83.7	-285.2	344.0	-113.0	BR	5.0	0.0	0.0	0.0
87.6	-289.2	349.6	-117.2	BR	5.0	0.0	0.0	0.0
97.3	-298.9	363.3	-120.0	BR	6.0	0.0	0.0	0.0
100.2	-301.8	367.4	-122.9	BR	5.0	0.0	0.0	0.0
103.0	-304.6	371.4	-123.3	GCBW	5.5	0.0 e	21.6	0.0
104.8	-314.4	381.3	-124.3	GCBW	7.0	1.0 e	27.2	0.0
106.5	-323.9	391.0	-126.6	GCBW	6.5	0.2 e	4.5	0.0
108.2	-333.6	400.9	-128.4	BR	5.0	0.0	0.0	0.0
109.0	-338.3	405.6	-129.9	GCB	5.0	0.0 e	4.1	0.0
109.9	-343.2	410.6	-129.9	GCB	5.0	0.5 e	4.6	0.0
110.9	-349.1	416.6	-130.8	BR	4.0	0.0	0.0	0.0
111.9	-354.9	422.5	-136.2	GCB	6.0	0.0 e	7.1	14.3
113.0	-360.8	428.5	-136.4	CB	4.5	0.7 e	10.0	0.0
114.7	-370.4	438.2	-138.5	BR	4.0	0.0	0.0	0.0
116.1	-378.5	446.4	-142.3	BR	3.5	0.0	0.0	0.0
117.7	-387.6	455.7	-146.1	CBW	3.5	0.0 e	1.3	0.0
118.7	-393.3	461.4	-147.7	CB	1.5	0.3 e	3.3	0.0
119.5	-398.0	466.3	-149.0	CB	4.0	0.4 e	5.2	0.0
120.3	-407.4	475.7	-152.3	CB	3.5	0.0 e	0.0	0.0
120.8	-412.2	480.5	-153.6	BR	1.5	0.0	0.0	0.0
121.4	-419.5	487.8	-158.9	BR		0.0	0.0	0.0
121.8	-424.4	492.7	-159.7	BR	2.5	0.0	0.0	0.0
122.5	-432.3	500.6	-160.8	GCBW	2.5	0.0 e	0.0	0.0
123.6	-445.1	513.5	-162.4	BR	5.0	0.0	0.0	0.0
124.5	-454.9	523.4	-164.4	BR	5.0	0.0	0.0	0.0
125.3	-464.6	533.1	-166.7	BR	6.0	0.0	0.0	0.0
126.2	-474.4	542.9	-168.7	BR	7.0	0.0	0.0	0.0
126.3	-475.7	544.3	-172.2	BR	2.0	0.0	0.0	0.0
127.2	-485.7	554.3	-172.2	BR		0.0	0.0	0.0
128.0	-495.2	563.8	-175.0	GCB	1.5	1.0 e	2.2	0.0
128.5	-500.2	568.8	-175.5	BR	1.0	0.0	0.0	0.0
128.8	-504.2	572.8	-178.5	BR	1.0	0.0	0.0	0.0
129.2	-508.5	577.1	-181.0	GCBW	1.0	0.0 e	0.0	0.0
129.6	-513.4	582.1	-180.8	BR	4.0	0.0	0.0	0.0
130.5	-523.9	592.6	-184.0	CB	1.5	0.0 e	1.1	0.0

upstream east-west coordinate (m) X	upstream north-south coordinate (m) Y	upstream length coordinate (m) L	upstream surface elevation (m) Z	section bed material M	upstream bed width (m) W	upstream bed depth (m) D	section bed volume (m^3) V_B	section sideslope volume (m^3) V_S
131.3	-532.8	601.6	-184.9	CB	2.0	0.2 e	3.4	0.0
132.2	-542.6	611.4	-186.7	GCB	2.2	0.3 e	9.6	0.0
133.0	-552.4	621.2	-188.8	GCB	6.0	0.4 e	20.9	0.0
133.9	-562.3	631.1	-189.8	GCBW	4.5	0.8 e	16.9	8.0
134.7	-572.0	640.9	-191.9	GCBW	3.5	0.5 e	32.8	10.0
135.6	-581.9	650.9	-192.5	GCB	5.5	1.6 e	56.7	0.0
136.5	-591.7	660.7	-194.5	GCBW	6.0	1.4 e	21.3	0.0
134.0	-600.9	670.2	-197.6	CBW	2.5	0.0 e	4.8	0.0
131.4	-610.5	680.1	-198.9	CBW	3.0	0.5 e	4.5	0.0
128.9	-619.8	689.7	-201.6	BR	2.5	0.0	0.0	0.0
126.4	-629.2	699.5	-203.8	GCB	3.5	0.0 e	33.0	0.0
123.8	-638.8	709.5	-203.2	GCB	4.5	2.4 e	76.1	0.0
121.2	-648.5	719.5	-203.6	CB	3.0	3.8 e	69.0	0.0
118.7	-657.9	729.2	-206.0	GCB	3.0	3.3 e	77.1	0.0
116.2	-667.5	739.1	-207.2	GCBW	3.5	3.9 e	103.3	0.0
113.6	-677.1	749.1	-208.5	CBW	4.0	4.4 e	81.8	0.0
111.2	-685.9	758.3	-212.4	GCB	4.0	2.2 e	27.2	0.0
109.6	-695.0	767.5	-216.3	BR	4.0	0.0	0.0	0.0
107.9	-704.7	777.3	-218.1	BR		0.0	0.0	0.0
106.2	-714.4	787.2	-219.6	CB	6.0	0.0 e	54.9	0.0
104.5	-724.3	797.2	-219.9	B	7.0	2.5 e	51.2	0.0
102.9	-733.1	806.1	-224.4	CB	4.0	0.5 e	3.7	0.0
102.2	-736.9	810.0	-227.6	GCB	2.5	0.4 e	2.7	0.0
101.4	-741.8	815.0	-227.7	CBW	1.5	0.4 e	2.2	0.0
99.7	-751.4	824.7	-230.1	BR	2.0	0.0	0.0	0.0
98.0	-761.1	834.6	-231.7	GCBW	4.0	0.0 e	2.1	0.0
97.1	-765.9	839.4	-233.0	GCBW	3.0	0.4 e	3.8	0.0
95.6	-774.7	848.3	-233.9	BR	3.5	0.0	0.0	0.0
94.8	-779.2	852.9	-237.8	GCBW	4.0	0.0 e	0.0	0.0
92.9	-789.8	863.7	-240.1	GCBW	4.0	0.0 e	2.4	0.0
92.0	-795.0	869.0	-243.9	GCBW	3.0	0.4 e	6.9	0.0
90.9	-801.4	875.4	-244.5	GCB	5.0	0.4 e	22.7	0.0
89.1	-811.2	885.4	-245.5	GCBW	5.0	1.0 e	20.7	0.0
87.4	-820.8	895.2	-247.6	GCB	5.0	0.3 e	18.5	0.0
85.7	-830.6	905.1	-248.5	GCBW	6.0	0.7 e	45.3	0.0
84.0	-840.4	915.1	-249.0	GCBW	4.0	2.1 e	17.4	0.0
82.9	-846.5	921.3	-252.3	GCBW	4.0	0.0 e	17.0	0.0
80.7	-859.0	934.0	-254.9	GCBW	4.0	1.0 e	22.6	0.0
79.3	-866.9	942.0	-255.5	BR	4.5	1.0	0.0	5.0
77.3	-878.3	953.5	-258.8	BR		0.0	0.0	5.0
75.6	-888.0	963.4	-260.2	BR		0.0	0.0	0.0
73.9	-897.5	973.0	-263.0	BR		0.0	0.0	0.0
72.2	-907.2	983.0	-264.1	BR		0.0	0.0	0.0
70.5	-917.0	992.9	-265.4	GCB		0.0 e	10.3	0.0
68.8	-926.5	1002.5	-268.1	GCB	12.0	0.4 e	32.3	0.0
67.1	-936.3	1012.5	-269.2	GCB	12.4	0.4 e	29.1	0.0
65.4	-945.9	1022.2	-271.4	GCB	10.0	0.4 e	36.0	0.0
63.6	-955.7	1032.2	-271.7	GCB	14.0	0.4 e	37.0	0.0
61.9	-965.5	1042.1	-272.9	GCB	14.0	0.4 e	31.7	0.0
60.2	-975.3	1052.0	-274.2	GCB	10.0	0.4 e	32.6	0.0
58.5	-985.1	1062.0	-274.9	GCB	14.5	0.4 e	35.2	0.0
56.7	-994.9	1072.0	-275.8	GCB	12.0	0.4 e	30.4	0.0
55.0	-1004.7	1081.9	-277.1	GCB	11.0	0.4 e	29.0	0.0
53.3	-1014.4	1091.8	-278.5	GCB	11.0	0.4 e	31.8	0.0
51.6	-1024.2	1101.7	-279.7	GCB	13.0	0.4 e	30.3	0.0
49.9	-1033.9	1111.6	-281.2	GCB	10.0	0.4 e	27.2	0.0

upstream east-west coordinate (m) X	upstream north-south coordinate (m) Y	upstream length coordinate (m) L	upstream surface elevation (m) Z	section bed material M	upstream bed width (m) W	upstream bed depth (m) D	section bed volume (m^3) V_B	section sideslope volume (m^3) V_S
48.2	-1043.5	1121.3	-283.6	GCB	11.0	0.4 e	29.9	0.0
46.4	-1053.3	1131.2	-284.8	GCB	11.6	0.4 e	33.3	0.0
49.8	-1062.6	1141.2	-286.0	GCB	13.5	0.4 e	37.1	0.0
53.2	-1071.9	1151.1	-287.3	GCB	14.6	0.4 e	32.6	0.0
56.6	-1081.3	1161.0	-288.5	GCB	10.0	0.4 e	27.9	0.0
60.0	-1090.6	1171.0	-289.5	GCB	11.0	0.4 e	26.5	0.0
63.4	-1099.9	1180.9	-290.5	GCB	9.0	0.4 e	23.9	0.0
66.8	-1109.3	1190.9	-291.5	GCB	9.0	0.4 e	23.7	0.0
70.2	-1118.6	1200.7	-293.1	GCB	9.0	0.4 e	23.9	0.0
73.6	-1127.9	1210.7	-293.9	GCB	9.0	0.4 e	23.2	0.0
77.0	-1137.2	1220.6	-295.4	GCB	8.6	0.4 e	22.9	0.0
80.4	-1146.6	1230.5	-296.6	GCB	8.7	0.4 e	18.2	5.0
83.8	-1155.9	1240.5	-297.5	GCB	5.0	0.4 e	14.6	0.0
87.2	-1165.3	1250.4	-298.5	GCB	6.0	0.4 e	15.5	10.0
90.5	-1174.4	1260.1	-301.0	GCB	6.0	0.4 e	18.6	10.0
93.9	-1183.7	1270.1	-302.1	GCB	8.0	0.4 e	23.1	10.0
97.3	-1193.0	1280.0	-303.4	GCB	9.5	0.4 e	26.0	15.0
100.7	-1202.2	1289.7	-305.5	GCB	10.4	0.4 e	27.2	0.0
107.1	-1209.9	1299.7	-305.7	GCB	10.0	0.4 e	22.0	90.0
113.5	-1217.5	1309.7	-306.8	GCB	6.6	0.4 e	18.1	90.0
119.9	-1225.1	1319.6	-307.7	GCB	7.0	0.4 e	16.5	120.0
126.3	-1232.8	1329.6	-308.2	GCB	5.4	0.4 e	13.8	0.0
128.9	-1242.4	1339.6	-308.8	GCB	5.0	0.4 e	10.7	3364.0
131.5	-1252.0	1349.6	-309.7	GCB	10.5	0.1 e	12.5	0.0
134.0	-1261.6	1359.5	-310.6	GCB	7.0	0.4 e	18.5	0.0
136.6	-1271.3	1369.5	-311.6	GCB	4.0	0.6 e	36.2	0.0
139.2	-1280.9	1379.5	-312.0	GCB	6.0	1.5 e	80.3	0.0
141.8	-1290.5	1389.4	-312.6	GCB	7.5	2.1 e	157.6	0.0
144.4	-1300.2	1399.4	-313.4	GCB	13.0	2.5 e	243.2	0.0
146.9	-1309.8	1409.4	-314.1	LJ	13.0	3.1 e	1699.6	0.0
143.8	-1327.4	1427.3	-312.3	LJ	39.0	7.2 e	2822.9	0.0
140.1	-1348.8	1449.0	-315.7	LJ	18.0	6.4 e	1309.9	0.0
135.8	-1373.0	1473.6	-320.5	LJ	10.5	4.7 e	129.2	0.0
135.0	-1377.4	1478.1	-322.7	LJ	12.0	3.0 e	22.0	0.0
134.7	-1379.2	1479.8	-326.0		13.0	0.0		

Approximate Geo-referencing Coordinates

	Survey Coordinates		UTM Zone 10, NAD27, meters		
creek ID	X	Y	X	Y	notes
HR 6	28.0	107.7	423980	5293740	right bank tributary (steep)
HR 4	106.9	675.1	421680	5294500	road crossing
HR 3	155.4	807.5	423220	5294860	road crossing
HR 2	-821.5	111.2	420040	5293530	road crossing
HR 1	-18.8	978.3	422160	5294580	road crossing
HR 5	13.6	875.6	427940	5293300	road crossing
WT	0.0	0.0	423760	5298430	colluvial tributary junction
ET	0.0	0.0	426090	5299140	large left bank slope failure
HBC	128.5	-106.2	422630	5298370	huge left bank slope failure
SP	146.9	-1309.8	419800	5304400	right bank logjam, new channel to left